

June 27, 2016

Dear Editor Dr. Dai,

Thank you very much for your comments on our last revision. We found your suggestions very helpful and have revised the manuscript accordingly. We have reduced the emphasis on the model as a tool for quantifying flux and clarified that the purpose of the two sensitivity tests (e.g. Exp2 and 3) was to examine coastal carbon cycle's sensitivity to different biological and riverine settings. Below please find our detailed response to your comments followed by a marked-up version of our revised manuscript. We believe our responses address your concerns and hope that you will find our revised manuscript acceptable for publication in *Biogeosciences*.

Sincerely,

Z. George Xue and co-authors

1) General comments:

While I am aware that this modeling effort is large and significant, and your validation shows overall good performance of the model, I would suggest to tune down the significance in quantifying the fluxes (throughout the MS but particularly in the introduction) and balance it with the community consensus that numerical model is a tool particularly compelling for process study. This is partially because the biogeochemical module is far from being realistic even though you have used realistic physical forcing.

Agree. We have reduced the emphasis on the model as a tool quantifying the fluxes throughout the MS as well as in the abstract. Instead, we have replaced the word “quantify” with “estimate” or “simulate” and also addressed that model was a tool mainly for process study.

2) Specific Comments:

2.1. abstract: Line 30-31: *“On average, the GoM was found to be a CO₂ sink with a flux of, which, together with the enormous fluvial carbon input, was balanced by the carbon export through the Loop Current”. This statement is not accurate. First of all, the form of carbon (organic vs inorganic) being referred here is unclear.Secondly, because of the involvement of the biological metabolism, CO₂ flux is actually balanced by the externally transported DIC plus the balance between DIC and nutrients metabolism (Dai et al., 2013, GRL).*

Agree. We replaced the word “balanced” with “comparable to”. We also indicated that our estimation here was for inorganic carbon. We added in the reference by Dai et al., 2013 as well as the relevant contents in the discussion (5.3).

3) About the model implantation:

3.1 P8, lines 173-175, *“Because direct riverine DIC measurements were not available, we approximated riverine DIC ...”, this has to be justified and the potential impact be evaluated as it is known pCO₂ is highly sensitive to DIC changes as indicated by the Revelle factor. Discussion about the uncertainties should be made if the approximate DIC has to be used.*

The estimation by Guo et al. (2012) that DIC roughly equals alkalinity plus 50 was based on several in-situ measurements in the channel. In addition, we re-examined all available measurements made by co-authors Cai, Lohrenz and Huang and derived a mean alkalinity of 1,980 mEq/L and a mean DIC of 2,015 $\mu\text{mol kg}^{-3}$ (45 data points in waters with salinity < 5). The mixing curve we derived using measured river and ocean-end members (Fig.1) indicated that

the mixing of riverine DIC was mainly in waters with a salinity below 25. Since our model cut off at the water depth of 5 m, less than 3 percent of the modeling domain had a salinity that is smaller than 25 (Fig.2). Also in MS Fig. 7, our simulated $p\text{CO}_2$ in low salinity waters fell between the two river end members, which demonstrated that our model setup was able to reproduce the $p\text{CO}_2$ condition in the coastal ocean. Nevertheless, we do agree that the $p\text{CO}_2$ in the Mississippi plume is very sensitive to river DIC inputs and added relevant discussion regarding our usage of riverine DIC in Section 5.3.

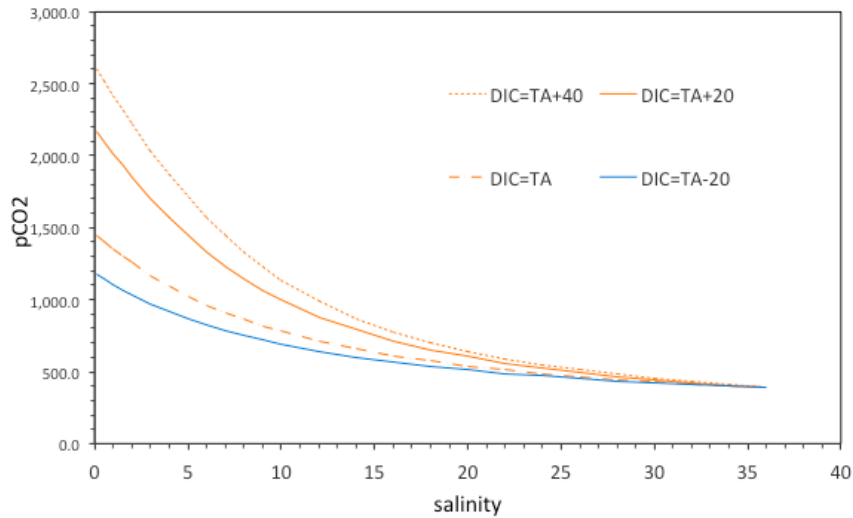


Fig 1. Mixing curve derived by in-situ measured river and ocean end members in the Northern Gulf of Mexico

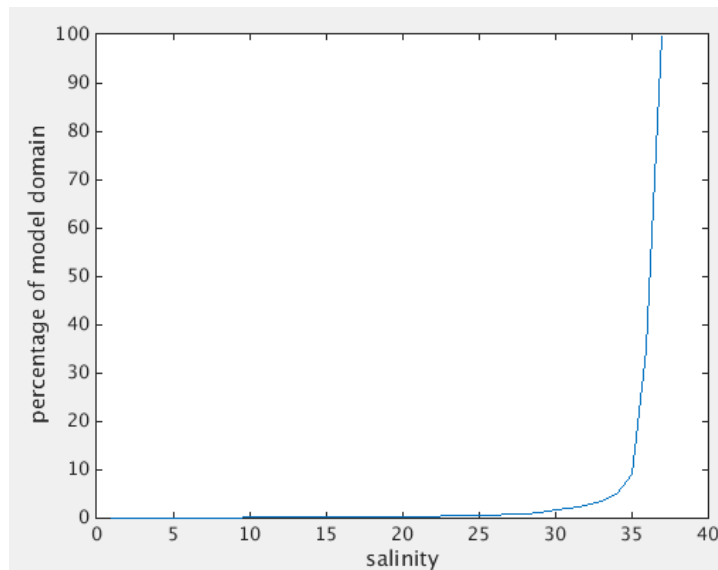


Fig.2 Salinity distribution over the model domain (2004-2010 mean)

3.2 P9, lines 181-183, "Experiment 2 (Exp2) was a "no-biology run", where all biological sources and sinks of DIC and alkalinity were disabled ...", disabling the biological sources and sinks of DIC and alkalinity can only reflect the biological effect qualitatively or quasi-quantitatively due to the non-linear relationship between them. Moreover, the biological effect interacts with other factors/processes such as temperature and air-sea flux, therefore, discussing the biological effect by disabling the biological process alone is not quite assuring.

Agree, we insert the word "qualitatively" as follows "The purpose of Exp2 was to qualitatively examine the role of biological processes in regulating regional pCO₂ variability..." (line 189-190). Same on p. 14, line 308 "To qualitatively test the role of ...".

3.3 P9, lines 183-186, "Experiment 3 ... the river inputs ... for the period of 1904-1910", except for the riverine input and air pCO₂, air temperature and seawater temperature also changed substantially during the last 100 years. Furthermore, the nutrient condition and carbonate system of the GoM may also have changed after 100 years' change in terrestrial input. Therefore, applying river input and air pCO₂ at that time and spin up for only 1 year is far from enough to simulate the coastal carbon dynamics a century ago.

Agree. In this experiment, our purpose was not to reproduce the 1904-1910 condition. Instead, we want to demonstrate the magnitude and spatial extent of coastal carbon's response to different river inputs condition. In line 206, we pointed out that "Exp 3 examined coastal carbon cycle's response to alternations in river inputs as a result of land-use change within the Mississippi watershed (the first ten years of the 20th century vs. that of the 21st century). Although we applied riverine and air pCO₂ estimated for the period of 1904-1910, the purpose of Exp3 was not to reproduce the pCO₂ for that period as changes of other variables over the past 100 years were not considered (e.g. air temperature, ocean and food web conditions)".

4 **Modeling $p\text{CO}_2$ Variability in the Gulf of Mexico**

5
6 Zuo (George) Xue^{1, 2, &3}, Ruoying He⁴, Katja Fennel⁵, Wei-Jun Cai⁶, Steven Lohrenz⁷,
7 Wen-Jen Huang⁸, Hanqin Tian⁹, Wei Ren¹⁰, Zhengchen Zang¹

- 8
9 1. Dept. of Oceanography and Coastal Sciences, Louisiana State University, Baton Rouge, LA, United States
10 2. Center for Computation and Technology, Louisiana State University, Baton Rouge, LA, United States
11 3. Coastal Studies Institute, Louisiana State University, Baton Rouge, LA, United States
12 4. Dept. of Marine, Earth & Atmospheric Sciences, North Carolina State University, Raleigh, NC, United States
13 5. Dept. of Oceanography, Dalhousie University, Halifax, Canada
14 6. School of Marine Science and Policy, University of Delaware, Newark, DE, United States
15 7. School for Marine Science and Technology, University of Massachusetts Dartmouth, New Bedford, MA,
16 United States
17 8. Department of Oceanography, National Sun Yat-sen University, Kaohsiung, Taiwan
18 9. School of Forestry and Wildlife Sciences, Auburn University, AL, United States
19 10. Department of Plant and Soil Sciences, University of Kentucky, Lexington, KY, United States
20
21

22 **Abstract**

23 A three-dimensional coupled physical-biogeochemical model was used to
24 simulate and examine temporal and spatial variability of sea surface $p\text{CO}_2$ in the Gulf of
25 Mexico (GoM). The model was driven by realistic atmospheric forcing, open boundary
26 conditions from a data-assimilative global ocean circulation model, and observed
27 freshwater and terrestrial nutrient and carbon input from major rivers. A seven-year
28 model hindcast (2004–2010) was performed and validated against ship measurements.
29 Model results revealed clear seasonality in surface $p\text{CO}_2$ and were used to estimate
30 carbon budgets in the Gulf. Based on the average of model simulations, the GoM was a
31 net CO_2 sink with a flux of $1.11 \pm 0.84 \times 10^{12} \text{ mol C yr}^{-1}$, which, together with the
32 enormous fluvial inorganic carbon input, was comparable to the inorganic carbon export
33 through the Loop Current. Two model sensitivity experiments were performed: one
34 without biological sources and sinks and the other using river input from the 1904-1910
35 period as simulated by the Dynamic Terrestrial Ecosystem Model (DLEM). It was found
36 that biological uptake was the primary driver making GoM an overall CO_2 sink and that
37 the carbon flux in the northern GoM was very susceptible to changes in river forcing.
38 Large uncertainties in model simulations warrant further process-based investigations.
39

Z. George Xue 7/1/2016 9:03 AM
Deleted: quantify

Z. George Xue 7/1/2016 9:03 AM
Deleted: compute

Z. George Xue 7/1/2016 9:03 AM
Deleted: On

Z. George Xue 7/1/2016 9:03 AM
Deleted: found to be

Z. George Xue 7/1/2016 9:03 AM
Deleted: balanced by

Z. George Xue 7/1/2016 9:03 AM
Deleted: sub-regional

Z. George Xue 7/1/2016 9:03 AM
Deleted: budget

Z. George Xue 7/1/2016 9:03 AM
Deleted: When the 1904-1910 river conditions were applied, the northern GoM became a CO_2 source instead.

50 **1. Introduction**

51 Human consumption of fossil fuels has resulted in continuously increasing levels
52 of atmospheric CO₂ since the Industrial Revolution began around 1750. If the increasing
53 trend continues, the projected $p\text{CO}_2$ by the end of the 21st century (970 ppm, in A1F1
54 scenario, [Stocker et al., 2014](#)) could be nearly triple the present level. In the face of
55 different climate scenarios, a better understanding of the oceans' role in regulating the
56 global carbon cycle is crucial, because oceans not only act as receivers of the enormous
57 carbon loading from coastal rivers ([Cai et al., 2011a](#); [Bauer et al. 2013](#)), but also as vast
58 carbon reservoirs via the “carbon pump” mechanism ([Sabine et al., 2004](#); [Sabine and](#)
59 [Tanhua, 2010](#)). On regional scales, the marine carbon cycle tends to be more complicated
60 and shows contrasting behaviors in different areas (coastal vs. open ocean, low latitude vs.
61 high latitude, etc.) and during different seasons (e.g., [Lohrenz et al., 2010](#) for the northern
62 Gulf of Mexico; [Jiang et al., 2008](#) for the South Atlantic Bight; [Signorini et al., 2013](#) for
63 the North American east coast; [Tsunogai et al., 1999](#) for the East China Sea). Quantifying
64 the ocean carbon budget is therefore a difficult task. Coupled physical and biological
65 models are useful tools for understanding complex biogeochemical processes and
66 estimating carbon and nutrient fluxes in coastal oceans where spatial and temporal
67 heterogeneities are high and data are sparse (e.g. [Fennel and Wilkin, 2009](#); [Fennel 2010](#);
68 [Fennel et al., 2011](#); and [He et al., 2011](#)).

69 Our study focuses on the carbon cycle in the Gulf of Mexico (GoM). One unique
70 feature of the Gulf is that it receives enormous riverine nutrient and carbon inputs, both
71 organic and inorganic, the majority of which are from the Mississippi-Atchafalaya River
72 system. Excessive nutrient loading causes coastal eutrophication, which triggers not only

73 the well-known hypoxia phenomenon (a.k.a. the “Dead Zone”, Rabalais et al., 2002), but
74 also a newly revealed coastal ocean acidification problem (Cai et al, 2011b). However,
75 the carbon cycling associated with such enormous terrestrial carbon and nutrient inputs
76 remains unclear: on the one hand extensive riverine carbon input results in CO₂ over-
77 saturation in coastal waters, which serve as a CO₂ source to the atmosphere (e.g. Lohrenz
78 et al., 2010; Guo et al., 2012); on the other hand, enhanced primary production in the
79 river plume due to significant inputs of inorganic nutrients induces a net influx of CO₂
80 although the Mississippi River Plume region is an overall heterotrophic system that
81 breaks down organic carbon (Murrell et al., 2013; Huang et al., 2013 and 2015). Further
82 offshore, the circulation in the GoM is largely influenced by the energetic Loop Current.
83 Large anticyclonic eddies aperiodically pinch off from the Loop Current (Sturges and
84 Leben, 2000), which, along with the wind-driven cross-shelf circulation and other meso-
85 scale and sub-mesoscale processes, enhance material exchanges between the eutrophic
86 coastal waters and oligotrophic deep-ocean waters (e.g., Toner et al., 2003). Indeed, a
87 recent observational study suggested a significant dissolved inorganic carbon export (DIC,
88 $\sim 3.30 \times 10^{12}$ mol C yr⁻¹) from the GoM shelves to the Loop Current waters (Wang et al.,
89 2013).

Z. George Xue 7/1/2016 9:03 AM

Deleted: budget

Z. George Xue 7/1/2016 9:03 AM

Deleted:), enhanced primary production in the river plume due to significant inputs of inorganic nutrients induces a net influx of CO₂.

90 While global inorganic carbon budgets have been made available through joint
91 seawater CO₂ observations (e.g. World Ocean Circulation Experiment and Joint Global
92 Ocean Flux study, Sabine et al., 2004; Feely et al., 2004; Orr et al., 2005), they are too
93 coarse to represent CO₂ variability in the GoM (Gledhill et al., 2008). Other recent efforts
94 were able to provide GoM sub-regional carbon assessments based on limited in situ
95 observations (e.g. Cai et al., 2003, Lohrenz et al., 2010, Huang et al., 2013, 2015a and

Z. George Xue 7/1/2016 9:03 AM

Formatted: Subscript

100 [2015b](#) focused on the Mississippi River plume and the Louisiana Shelf; [Wang et al., 2013](#)
101 covered three cross-shelf transects in the northeastern GoM but only for one summer).
102 Significant uncertainties exist in such budget estimations due to large temporal and
103 spatial gaps presented in the observations (e.g. [Coble et al., 2010](#); [Hofmann et al., 2011](#);
104 [Robbins et al., 2014](#)). In this regard, coupled physical-biogeochemical models are
105 capable of representing the biogeochemical cycle with realistic physical settings (e.g.,
106 ocean mixing and advection) and providing an alternative means for a Gulf-wide carbon
107 budget estimation.

108 Here we present a GoM $p\text{CO}_2$ analysis based on the results of a coupled physical-
109 biogeochemical model simulation. Our objective was to simulate the CO_2 flux at the air-
110 sea interface (which at present is based on observational analyses alone and subject to
111 large uncertainty), as well as its variability in relationship with river plume dynamics and
112 dominant oceanic processes in different regions of the GoM.

113

114 2. Method

115 Our analysis uses solutions from a coupled physical-biogeochemical model
116 covering the GoM and South Atlantic Bight waters ([Xue et al., 2013](#), model domain see
117 [Fig.1](#)). The circulation component of the coupled model is the Regional Ocean Modeling
118 System (ROMS, [Haidvogel et al. 2008](#), [Shchepetkin and McWilliams, 2005](#); [Hyun and](#)
119 [He, 2010](#)) and is coupled with the biogeochemical module described in [Fennel et al.](#)
120 [\(2006, 2008, and 2011\)](#). The nitrogen cycling parameterization has seven state variables:
121 two species of dissolved inorganic nitrogen (DIN hereafter, nitrate $[\text{NO}_3]$ and ammonium
122 $[\text{NH}_4]$), one functional phytoplankton group, chlorophyll as a separate state variable to

Z. George Xue 7/1/2016 9:03 AM

Deleted: assessment

Z. George Xue 7/1/2016 9:03 AM

Deleted: is

Z. George Xue 7/1/2016 9:03 AM

Deleted: quantify

126 allow for photoacclimation, one functional zooplankton group, and two pools of detritus
127 representing large, fast-sinking particles, and suspended, small particles. The carbon
128 cycle is connected to the nitrogen cycle via a C to N ratio of 6.625 for the organic
129 components (phytoplankton, zooplankton, large and small detritus). The sediment
130 component of the biogeochemical model is a simplified representation of benthic
131 remineralization processes, where the flux of sinking organic matter out of the
132 bottommost grid box results immediately in a corresponding influx of ammonium and
133 DIC at the sediment/water interface. The parameterization accounts for the loss of fixed
134 nitrogen through sediment denitrification based on the linear relationship between
135 sediment oxygen consumption and denitrification reported by [Seitzinger and Giblin](#)
136 [\(1996\)](#) and only accounts for the portion of denitrification that is supported by
137 nitrification of ammonium in the sediment (referred to as coupled
138 nitrification/denitrification).

139 A seven-year (January 1, 2004–December 31, 2010) model hindcast was
140 performed, driven by NCEP’s high resolution combined model and assimilated
141 atmospheric dataset ([North American Regional Reanalysis, www.cdc.noaa.gov](#)), open
142 boundary conditions for ocean model (temperature, salinity, water level, and velocity)
143 from a data-assimilative global ocean circulation model (HYCOM/NCODA, [Chassignet](#)
144 [et al., 2007](#)), and observed freshwater and terrestrial nutrient input from 63 major rivers
145 ([Aulenbach et al., 2007](#); [Milliman and Farnsworth, 2011](#); [Fuentes-Yaco et al., 2001](#); and
146 [Nixon, 1996](#)). Model validations (physics, nutrients and chlorophyll) and a nitrogen
147 budget were reported in [Xue et al. \(2013\)](#).

148 In this study, we have focused on the carbon cycle in the GoM. As in [Xue et al.](#)
149 [\(2013\)](#), we considered the first year of the simulation (2004) as model spin-up; all results
150 presented here use model output from 2005 to 2010. The carbonate chemistry of the
151 coupled model is based on the standard defined by the Ocean Carbon Cycle Model
152 Intercomparison Project Phase 2 ([Orr et al., 2000](#)). There are two active tracers, DIC and
153 alkalinity, to determine the other four variables of the carbonate system (i.e. $p\text{CO}_2$,
154 carbonate ion concentration, bicarbonate ion concentration, and pH; [Zeebe and Wolf-](#)
155 [Gladrow, 2001](#)). Details of the formulas used in the simulation are provided in the
156 supplementary materials S1.

157 Similar to the results reported by [Hofmann et al. \(2011\)](#), we found that the model-
158 simulated DIC concentration in the water column was very sensitive to the initial
159 conditions. Although there were many historical measurements in the GoM, these data
160 were limited to the northern GoM shelf regions and thus were insufficient to initialize the
161 model. Instead, we tested model sensitivity using three sets of initial and open boundary
162 conditions, which were derived using the empirical salinity-temperature-DIC-alkalinity
163 relationships described in [Lee et al. \(2000 and 2006\)](#), [Cai et al. \(2011a\)](#), and [Wang et al.](#)
164 [\(2013\)](#), respectively. Among them, the initial condition prescribed following [Lee et al.](#)
165 [\(2000 and 2006, Fig.2, details see supplementary materials S2\)](#) provided the best model-
166 data comparison. For the open boundary condition, we found simulated surface $p\text{CO}_2$
167 exhibited very limited variance (<5%) regardless of which conditions were applied. To be
168 consistent with the setup of the initial condition, the results presented here were driven by
169 boundary conditions derived from [Lee et al., \(2000 and 2006\)](#). For particular organic

Z. George Xue 7/1/2016 9:03 AM

Deleted: are

Z. George Xue 7/1/2016 9:03 AM

Deleted: are

Z. George Xue 7/1/2016 9:03 AM

Deleted: are

173 carbon, we set a small, positive value for both phytoplankton and zooplankton along the
174 open boundaries.

175 The carbon cycle parameterizations used in this study followed the same approach
176 and values as in Fennel et al. (2008), Fennel and Wilkin (2009), and Fennel (2010). For
177 gas exchange calculations we followed the formulas in Wanninkhof (1992, details see
178 supplementary materials S3). For air pCO_2 , we utilized the Atmospheric Infrared Sounder
179 (AIRS, 2008) monthly gridded observation dataset and averaged them over the study area.
180 We applied the curve-fitting method using a C language program named CCGCRV
181 (<http://www.esrl.noaa.gov/gmd/ccgg/mbl/crvfit/crvfit.html>, Fig.3), and the air pCO_2 in
182 the gas exchange calculation was prescribed as:

183

$$184 \quad pCO_{2air} = D0 + D1*t + D2*(t^2) + D3*\sin(pi2*t) + D4*\cos(pi2*t) \\ 185 \quad + D5*\sin(pi2*2*t) + D6*\cos(pi2*2*t) \quad (1)$$

186 where pCO_{2air} represents the monthly air pCO_2 ; t represents the number of months since
187 January 2004 divided by 12, $pi2$ is a constant set to 6.28, $D0=375.96$, $D1=2.23$, $D2=-$
188 0.007 , $D3=1.31$, $D4=-0.64$, $D5=-0.13$, $D6=0.21$, and $D7=0.09$. Due to the relatively low
189 horizontal resolution of the AIRS data (2.5*2 degree), air pCO_2 was set to be spatially
190 uniform.

191 To account for riverine inputs, we constructed climatological monthly alkalinity
192 time series by averaging all available U.S. Geological Survey (USGS) observations for
193 each major river, including the Mississippi, Atchafalaya, Mobile, and Brazos in the GoM.
194 Because direct riverine DIC measurements were not available, we approximated riverine
195 DIC inputs using the corresponding alkalinity value plus 50, following the observational

196 study by Guo et al. (2012). The fluvial DIC input to the GoM was estimated as $\sim 2.18 \times$
197 10^{12} mol C yr⁻¹, the majority of which was delivered by the Mississippi-Atchafalaya
198 River ($\sim 1.80 \times 10^{12}$ mol C yr⁻¹, Fig.4, comparable with the estimation in Cai et al., 2003).

199 The results of three model experiments covering the period of 2004-2010 are
200 presented in this study, in which, Experiment 1 (Exp1) was a “control run”, with
201 observed riverine inputs from USGS and biological sources and sinks of DIC and
202 alkalinity in the water column; Experiment 2 (Exp2) was a “no-biology run”, where all
203 biological sources and sinks of DIC and alkalinity were disabled, similar to the
204 experiment described in Fennel and Wilkin (2009); and Experiment 3 (Exp3) had the
205 same set up as Exp1, but the riverine inputs (water, nutrients, and carbon of the
206 Mississippi-Atchafalaya river) were taken from the Dynamic Land Ecosystem Model
207 (DLEM, Tian et al., 2015) simulation for the period of 1904-1910 (Fig. 4). Specifically,
208 we used the monthly model outputs of water, NO₃, NH₄, and alkalinity from DLEM as
209 riverine inputs to drive the ocean model in Exp1. Also in Exp3 the air pCO₂ was set to
210 the 1904-1910 condition derived by formula (1). The purpose of Exp2 was to
211 qualitatively examine the role of biological processes in regulating regional pCO₂
212 variability, whereas Exp3 examined the coastal carbon cycle’s response to alternations in
213 river inputs as a result of land-use change within the Mississippi watershed (the first ten
214 years of the 20th century vs. that of the 21st century). Although we applied riverine and
215 air pCO₂ estimated for the period of 1904-1910, the purpose of Exp3 was not to
216 reproduce the pCO₂ for that period as changes of other variables over the past 100 years
217 were not considered (e.g. air temperature, ocean and food web conditions).

218

Z. George Xue 7/1/2016 9:03 AM

Deleted: connections between variability of

Z. George Xue 7/1/2016 9:03 AM

Deleted: dynamics and historical climate

Z. George Xue 7/1/2016 9:03 AM

Deleted: and land-use

Z. George Xue 7/1/2016 9:03 AM

Deleted: within the Mississippi watershed.

Z. George Xue 7/1/2016 9:03 AM

Formatted: Indent: First line: 0"

223

224 3. Validation of the control run

225 We utilized the ship-based sea surface $p\text{CO}_2$ database compiled by the Lamont-
226 Doherty Earth Observatory (LDEO Version 2014, >180,000 data points in the Gulf over
227 2005-2010, [Takahashi et al., 2015](#)) and [Huang et al. \(2015a and b\)](#) for model validation
228 (see locations of ship measurements in [Fig.5](#)). The ship measurements by [Huang et al.](#)
229 [\(2015a and b\)](#) were taken in October 2005; April, June, August 2006; May, August 2007;
230 January, April, July, November 2009; and March 2010, respectively and contain > 78,000
231 data points. To alleviate the spatial and temporal mismatches associated with these in-situ
232 measurements, we computed their temporal and spatial mean using a 10-day temporal
233 binning for temporal processing, and then compared them with model-simulated $p\text{CO}_2$
234 time series ([Fig.6](#)). To facilitate our analysis, the GoM was divided into five sub-regions:
235 1) Mexico Shelf (MX Shelf), 2) West Gulf of Mexico Shelf (WGoM Shelf), 3) Northern
236 Gulf of Mexico Shelf (NGoM Shelf), 4) West Florida Shelf (WF Shelf), and 5) the open
237 ocean, which is > 200m water depth (regional definitions followed [Benway and Coble,](#)
238 [2014](#), maps of sub-regions see [Fig.1](#)). The data points falling in each of the sub-regions
239 was first grouped by a 10-day temporal binning and then spatially averaged to get a mean
240 value for each sub-region.

241 On the NGoM Shelf, the control simulation was able to capture the measured
242 $p\text{CO}_2$ in 21 out of the 26 data groups (the mean value of in-situ measurements fell within
243 one standard deviation of the model mean). Specifically, agreement between model and
244 observations was better during spring, fall, and winter, than during summer. The model
245 overestimated $p\text{CO}_2$ in June 2006, August 2007, and July 2009. These discrepancies will

246 be discussed in later sections. On the Gulf-wide scale, the control run reproduced the
247 observed seasonality. Decent model-data agreements were found in 24 out of the 26 data
248 groups. These sub-regional and Gulf-wide comparisons indicate that the coupled
249 physical-biogeochemical model is generally capable of resolving temporal and spatial
250 variations in observed $p\text{CO}_2$, allowing us to use this seven-year hindcast to further
251 characterize the air-sea CO_2 flux.

252

253 4. Results

254 In this section, we present model-simulated sea surface $p\text{CO}_2$ and air-sea CO_2 flux
255 in the five sub-regions. Because few data existed and large $p\text{CO}_2$ gradients were found in
256 both in-situ measurements and model simulation in shallow waters, areas that are
257 shallower than 10 m were excluded from our analysis.

258 4.1 Temporal variability of Sea Surface $p\text{CO}_2$

259 Spatially averaged model-simulated $p\text{CO}_2$ on the NGoM Shelf exhibited clear
260 seasonality, with highest values (~ 500 ppm) around August and lowest values (~ 300
261 ppm) around February (Fig.6a). Notably, spatially averaged $p\text{CO}_2$ on the NGoM Shelf
262 was not coincident with high river carbon and nutrient inputs (Fig.3). Peaks in $p\text{CO}_2$
263 generally occurred two to three months later than the annual maximum in river input. The
264 maximum riverine input during 2005-2010 was observed in June 2008 when a major
265 flood occurred (Fig. 4a), yet no significant elevation of $p\text{CO}_2$ was seen in the model
266 simulation. Gulf-wide spatially averaged $p\text{CO}_2$ (Fig.4b) had a temporal pattern similar to
267 that on the NGoM Shelf, with high $p\text{CO}_2$ values (~ 425 ppm) in August and low values

Z. George Xue 7/1/2016 9:03 AM

Formatted: Font:Bold

Z. George Xue 7/1/2016 9:03 AM

Deleted: -

Z. George Xue 7/1/2016 9:03 AM

Deleted: large

Z. George Xue 7/1/2016 9:03 AM

Deleted: smallest

Z. George Xue 7/1/2016 9:03 AM

Deleted: were

Z. George Xue 7/1/2016 9:03 AM

Deleted: simulated

273 (~ 350 ppm) in February. Averaged $p\text{CO}_2$ on the NGoM Shelf was generally 50 ppm
274 higher than that in the entire Gulf.

275 **4.2 Model Simulations of Air-Sea CO_2 flux**

276 The simulated carbon flux was calculated from a multi-year model mean (2005-
277 2010). We found that the GoM overall was a CO_2 sink with a mean flux rate of 0.71 ± 0.54
278 $\text{mol C m}^{-2} \text{ yr}^{-1}$ ($\sim 1.11 \pm 0.84 \times 10^{12} \text{ mol C yr}^{-1}$, Table 1 and Fig.7). Examining region by
279 region, we found that the open ocean, occupying ~ 65% of the GoM by area, acted as a
280 CO_2 sink ($1.04 \pm 0.46 \text{ mol m}^{-2} \text{ yr}^{-1}$ of C) during most of the year except in summer. The
281 greatest carbon uptake occurred in winter ($2.44 \pm 0.49 \text{ mol C m}^{-2} \text{ yr}^{-1}$). It is evident that
282 waters around the Loop Current act as a sink throughout the year, whereas the western
283 part of the open ocean waters shifted from acting as a CO_2 source in summer and fall to a
284 sink in winter and spring.

285 Compared with the open ocean, air-sea flux on the continental shelf was more
286 location-dependent and varied from season to season. Among the four shelf sub-regions,
287 the MX Shelf has the largest area. It acted as a strong CO_2 sink in winter and spring
288 (0.49 ± 0.28 and $0.97 \pm 0.28 \text{ mol C m}^{-2} \text{ yr}^{-1}$) and then a carbon source in summer and fall (-
289 0.96 ± 0.38 and $-0.76 \pm 0.45 \text{ mol C m}^{-2} \text{ yr}^{-1}$). Waters along the eastern side of the MX Shelf
290 were a sink during most of the year, while to the west the shelf was a source in summer
291 and fall. On an annual scale, this region was a sink with an air-sea flux of $0.19 \pm 0.35 \text{ mol}$
292 $\text{C m}^{-2} \text{ yr}^{-1}$. To the north, the WGoM Shelf has the smallest area among the four shelf sub-
293 regions. It acted as a CO_2 source during spring, summer, and fall (-0.24 ± 0.59 , -1.69 ± 0.43
294 and $-1.06 \pm 0.34 \text{ mol C m}^{-2} \text{ yr}^{-1}$) and a strong CO_2 sink during winter ($1.62 \pm 0.32 \text{ mol C m}^{-2}$

Z. George Xue 7/1/2016 9:03 AM

Deleted: -

... (1)

297 yr⁻¹). On an annual scale the WGoM region was a CO₂ source with a degassing rate of
298 0.34±0.42 mol C m⁻² yr⁻¹.

299 The NGoM Shelf shifted from acting as a CO₂ source in summer and fall (-
300 1.42±0.74 and -0.79±0.63 mol C m⁻² yr⁻¹) to a sink in winter and spring (1.01±0.89 and
301 2.49±0.70 mol C m⁻² yr⁻¹). The most prominent feature here was the continuous, strong
302 degassing in the coastal waters around the Mississippi-Atchafalaya River mouths.
303 However, as the water becomes deeper, the NGoM Shelf water shifted from acting as a
304 sink during winter and spring to a source during summer and fall. Despite of the
305 extensive degassing in the coastal water, the NGoM Shelf overall was a CO₂ sink on a
306 yearly basis (0.32±0.74 mol C m⁻² yr⁻¹). Similarly, the WF Shelf also shifted from acting
307 as a CO₂ source in summer and fall (-1.26±0.53 and -1.73±0.67 mol C m⁻² yr⁻¹) to a sink
308 in winter and spring (1.19±0.38 and 0.28±0.33 mol C m⁻² yr⁻¹). The degassing in the inner
309 shelf was strong enough to make the WF Shelf a CO₂ source on a yearly basis (-
310 0.38±0.48 mol C m⁻² yr⁻¹).

311 Despite the salient spatial and temporal variability, the GoM was an overall CO₂
312 sink, mainly because of the strong uptake in the open ocean. For validation purposes, we
313 compared (in [Table 1](#)) model-simulated air-sea flux against an estimation based on
314 observations, which utilized all available measurements collected within the GoM from
315 2005 to 2010 ([Robbins et al., 2014](#)). Our control-run estimations generally agree with in-
316 situ measurements in all five sub-regions in terms of the ocean's role as a CO₂ source or
317 sink. There is some discrepancy in the magnitude of the estimated flux, specifically in the
318 Open Ocean sub-region. We note that [Robbins et al. \(2014\)](#) used monthly mean *p*CO₂
319 and wind fields in their calculation as opposed to the 10-day interval we used here.

320 Therefore, to facilitate the comparison of results, we recalculated the flux using a
321 monthly mean $p\text{CO}_2$ and wind fields and obtained a flux estimate of $0.31 \pm 0.35 \text{ mol C m}^{-2}$
322 yr^{-1} for the Open Ocean sub-region, and $0.12 \pm 0.23 \text{ mol C m}^{-2} \text{ yr}^{-1}$ for the entire GoM.
323 These values are comparable to those in [Robbins et al. \(2014\)](#), $0.48 \pm 0.07 \text{ mol C m}^{-2} \text{ yr}^{-1}$
324 for the Open Ocean and $0.19 \pm 0.08 \text{ mol C m}^{-2} \text{ yr}^{-1}$ for the entire GoM).

325 **4.3 Net Community Production**

326 As Net Community Production (NCP) plays an important role in regulating water
327 CO_2 concentration, we generated maps of seasonal mean surface NCP as well as time
328 series of spatially averaged surface NCP for the NGoM and Open Ocean in [Figs. 8 and 9](#).
329 High NCP was simulated in the surface NGoM water and near the eastern tip of the MX
330 shelf during most time of the year. For the NGoM shelf, surface NCP peaks in the late
331 spring and early summer, with the highest value (2.62 mmol N/m^3) simulated in summer
332 2008 when there was a major flooding event. Compared with the NGoM condition (0.53
333 mmol N/m^3), mean surface NCP in the Open Ocean was relatively small, with a multi-
334 year mean value of 0.11 mmol N/m^3 . In addition, the Gulf-wide mean surface NCP
335 exhibited peaks in late winter and early spring, mainly incurred by the strong upwelling
336 along the west side of the Yucatan Strait ([Figs. 8a and 8d](#)). Compared with the surface
337 NCP, the magnitude of bottom NCP was found to be small, and is thus not shown.

338 **4.4 Model Sensitivity experiments: No-biology simulation (Exp2)**

339 To qualitatively test the role of biological processes in regional CO_2 variability, a
340 no-biology run was conducted, where all biology sources and sinks of DIC and alkalinity
341 were disabled similar to the experiment described in [Fennel and Wilkin \(2009\)](#). The
342 experiment produced higher surface $p\text{CO}_2$ than the control run. $p\text{CO}_2$ is strongly elevated

Z. George Xue 7/1/2016 9:03 AM

Deleted: -

Z. George Xue 7/1/2016 9:03 AM

Deleted: for

Z. George Xue 7/1/2016 9:03 AM

Deleted: (0.05 mmol N/m^3 for the NGoM)

Z. George Xue 7/1/2016 9:03 AM

Deleted: -

Z. George Xue 7/1/2016 9:03 AM

Formatted: Subscript

347 around the Mississippi River Delta on the NGoM shelf during spring and summer. For
348 the Open Ocean, the $p\text{CO}_2$ increase was mainly confined within the loop current and was
349 strongly impacted by Caribbean waters flowing in through the Yucatan Channel (Fig. 10).
350 To assess the influence of NCP on CO_2 variation, we plotted the $p\text{CO}_2$ difference between
351 the Control run (Exp1) and No-biology run (Exp2) against the surface NCP from the
352 Control run in Fig. 11. In the NGoM, the $p\text{CO}_2$ difference between the Control run and
353 No-biology run was strongly correlated with NCP ($r=0.80$), indicating a regional
354 biological carbon removal. For the Open Ocean, the $p\text{CO}_2$ difference shows no
355 correlation with NCP, and we speculate that the biological carbon removal in this region
356 was incurred not only by local NCP, but also remote processes. As shown in Fig. 9, the
357 poor correlation between $p\text{CO}_2$ and local NCP could be the result of the high $p\text{CO}_2$ water
358 from the Caribbean, which will be discussed in Section 5.2.

359 The multi-year mean sea surface $p\text{CO}_2$ from the no-biology run was elevated by
360 88.0 ppm (from 393.1 to 466.5 ppm) for the NGoM Shelf and 56.0 ppm (from 375.1 to
361 463.1 ppm) for the entire Gulf (Fig. 6, spatially averaged over the sub-regions). This
362 $p\text{CO}_2$ increase was not temporally uniform. On the NGoM Shelf, $p\text{CO}_2$ increases in the
363 no-biology run were clearly higher during spring-summer (with increases of 84.1 and
364 95.6 ppm) than during fall-winter (with increases of 57.3 and 56.0 ppm). On the Gulf-
365 wide scale, the $p\text{CO}_2$ increase was stronger during summer (97.1 ppm) than the other
366 seasons (86.5, 87.6, and 80.9 ppm for spring, fall, and winter). For air-sea flux, the
367 elevated surface $p\text{CO}_2$ turns all five sub-regions into a carbon source throughout the year,
368 resulting in a net outflux rate of $2.10 \text{ mol C m}^{-2} \text{ yr}^{-1}$ (Table 1).

369 4.5 Model Sensitivity experiments: historical river forcing (Exp3)

Z. George Xue 7/1/2016 9:03 AM

Deleted: 09

Z. George Xue 7/1/2016 9:03 AM

Deleted: .

372 | The purpose of Exp3 was to examine coastal carbon dynamics' response to
373 | different river conditions. Fig.4 shows that river discharge and DIC inputs during years
374 | 1904-1910 as simulated by the DLEM model are comparable with those at present (2004-
375 | 2010). The multi-year mean value of freshwater discharge is 25,700 m³/s for 1904-1910
376 | and 23,900 m³/s for 2004-2010. The Mississippi-Atchafalaya delivered 1.51×10¹² mol C
377 | yr⁻¹ during 1904-1910 and 1.70×10¹² mol C yr⁻¹ during 2004-2010, which is comparable
378 | to the increase over the preceding century reported by Raymond et al. (2008), i.e., a 0.24
379 | ×10¹² mol C yr⁻¹ increase in an average discharge year. However, NO₃ inputs during
380 | 1904-1910 were < 30% of current inputs (18.12 vs. 63.18 ×10⁹ mol N yr⁻¹). Limited N
381 | input led to a smaller primary production not only on the NGoM Shelf, but also the
382 | adjacent waters on the WGoM and WF Shelves. Due to the smaller primary production
383 | the coastal ocean was a weaker CO₂ sink during spring and summer (Fig. 12) and the
384 | NGoM Shelf a year-long carbon source with a net outflux rate of 0.61 mol C m⁻² yr⁻¹
385 | (Table 1). A close examination of the spring and summer conditions on the NGoM Shelf
386 | shows that differences in primary production between Exp1 and Exp3 occur mainly along
387 | the Texas and Louisiana coasts. Primary production was significantly elevated in the
388 | control run because of enhanced NO₃ inputs (Fig. 12a and c). Elevated primary
389 | production brought down the sea surface pCO₂. During spring, enhanced primary
390 | production and decreased CO₂ was simulated along the Louisiana and Texas coast (Fig.
391 | 12b), while during summer, when coastal circulation was influenced by westerly winds,
392 | the decreased pCO₂ was more confined within waters along the Louisiana coast.

393 |
394 | **5. Discussion**

Z. George Xue 7/1/2016 9:03 AM

Deleted: .

Z. George Xue 7/1/2016 9:03 AM

Deleted: .

397 Prior to this investigation, the carbon dynamics in the GoM have been poorly
398 characterized and had a high degree of uncertainty. This study provides one of the first
399 attempts to simulate GoM-wide carbon fluxes and exchanges using a coupled physical-
400 biogeochemical model. We next discuss the factors controlling sea surface $p\text{CO}_2$
401 variability on the river-influenced NGoM Shelf and the Loop Current-influenced open
402 ocean. The relationship between $p\text{CO}_2$ and other hydrographic variables as well as model
403 uncertainty are also considered.

Z. George Xue 7/1/2016 9:03 AM

Deleted: quantify

404 **5.1 NGoM Shelf**

405 The Mississippi-Atchafalaya River and associated plume play the most important
406 role in determining the $p\text{CO}_2$ distribution on the NGoM Shelf. The large input of fluvial
407 DIC and alkalinity introduces carbonate saturation in the coastal waters, conversely,
408 nutrients from the river enhance local primary production, which results in DIC removal
409 and thus reduces sea surface $p\text{CO}_2$ (e.g. [Lohrenz et al., 2010](#); [Guo et al., 2012](#); [Huang et
410 al., 2013 and 2015](#)). Such biological removal of CO_2 was also confirmed by the elevated
411 $p\text{CO}_2$ values in the no-biology run in this study. Although the river plume's influence on
412 CO_2 flux has been addressed by prior observational studies, large uncertainties were also
413 found regarding whether the NGoM Shelf is a CO_2 sink or source over a longer time
414 period. For instance, [Huang et al. \(2013\)](#) found a large difference between the $p\text{CO}_2$
415 distributions in April 2009 and in March 2010. Such a difference was attributed to the
416 variations in river plume extension influenced by local wind conditions and river
417 discharge. In a later communication, based on ship-measurements from 11 cruises, [Huang
418 et al. \(2015a\)](#) concluded that the NGoM Shelf acted as a net CO_2 sink, but with a large
419 uncertainty (influx rate: $0.96 \pm 3.7 \text{ mol m}^{-2} \text{ yr}^{-1}$).

Z. George Xue 7/1/2016 9:03 AM

Deleted: .

422 Model results in this study revealed significant spatial and temporal gradients in
423 sea surface $p\text{CO}_2$ as well. The multi-year mean (2005-2010) $p\text{CO}_2$ distribution was
424 characterized by high values in the coastal waters (Fig. 13a), accompanied by low salinity
425 (Fig. 13c), high Dissolved Inorganic Nitrogen (DIN) and high DIC (Figs. 13d and 13e).
426 The $p\text{CO}_2$ value was significantly lower as water became deeper, where the ocean acted
427 as a CO_2 sink during most times of the year (Figs. 7a through d). The surface $p\text{CO}_2$
428 distribution on the NGoM Shelf was highly correlated with surface salinity (r value: -0.81)
429 and DIN concentration (r value: 0.80) throughout the year, while its correlations with
430 surface temperature and DIC concentration were significant only for part of the year (for
431 detailed season-by-season correlations see Table 2). Although our model suggests that the
432 shelf-wide $p\text{CO}_2$ distribution was positively correlated with DIN concentration, this is not
433 contrary to findings of the above-mentioned observational studies, that is, the high DIN
434 stimulates primary production should be negatively correlated with sea surface $p\text{CO}_2$.
435 Instead, the high DIN concentration, together with the low salinity, was a signal of rich
436 DIC from the riverine inputs and, potentially, the light-limited conditions due to the high
437 suspended sediment and dissolved organic matter concentrations within the river plume.
438 In other words, CO_2 outgassing from oversaturated plume water overwhelmed the CO_2
439 influx induced by “biological pump” in the areas near the river mouths.

440 To further link $p\text{CO}_2$ dynamics with biological processes stimulated by river
441 inputs, we plotted the $p\text{CO}_2$ and DIC averaged over spring and summer seasons (high
442 flow from the Mississippi) against surface salinity of the control run and no-biology run
443 in Fig. 14. Seawater $p\text{CO}_2$ decreased almost linearly as salinity increased in the no-
444 biology run (Fig. 14b). During spring and summer when river discharge and DIC inputs

445 were high, the high $p\text{CO}_2$ and low salinity waters around the Mississippi River Delta (86-
446 88°W, reddish points) can be easily differentiated from the high salinity and low $p\text{CO}_2$
447 waters on the Texas Shelf (92-95°W, bluish points). The DIC-salinity relationship for
448 waters around the Mississippi Delta (reddish points in Fig. 14d) fell below the
449 conservative mixing relationship for the river end member calculated using in-situ data
450 collected in the spring and summer of 2008 by Cai et al. (2011a). For locations to the
451 west, the DIC-salinity relationship reflected a mixture of waters from the Texas shelf
452 (bluish points) and those from the Atchafalaya river (yellowish-greenish points) likely
453 with differing end members.

454 When biological processes were included, the shelf water exhibited large spatial
455 and seasonal variability (left panels). A $p\text{CO}_2$ minimum was simulated in mid-salinity
456 waters (30-33 psu) during spring and summer, which is consistent with the curve derived
457 by Huang et al., 2015a using ship measurements. Compared with the no-biology run,
458 $p\text{CO}_2$ was reduced significantly and exhibited a wider range in the control run. The
459 biological removal of sea surface CO_2 was most salient in waters around the Mississippi
460 River Delta. The difference in $p\text{CO}_2$ between waters around the delta and the Texas Shelf
461 became more salient. The DIC-salinity relationship for locations around the Mississippi
462 River delta (reddish points in Fig. 14c) indicated a significant carbon removal along the
463 salinity gradient. For waters on the Texas Shelf, the DIC-salinity relationship was
464 confined to higher salinities and slightly increased compared with the no-biology run
465 (bluish points in Fig.14c). The DIC increase on the Texas Shelf in the control run could
466 be linked with the benthic respiration in this region proposed by Hetland and DiMarco
467 (2007).

Z. George Xue 7/1/2016 9:03 AM
Formatted: Font:Bold

468

469

470 5.2 Open Ocean

471 In the open ocean, the distribution of surface $p\text{CO}_2$ was strongly related to the
472 surface DIC (r value: 0.93) and alkalinity throughout the year (r value: -0.85, for
473 detailed season-by-season correlations see [Table 2](#)). An influence of DIN and primary
474 production was evident in fall and winter months when wind-induced upwelling was
475 strong ([Xue et al., 2013](#)). The dependence of $p\text{CO}_2$ on DIC and alkalinity makes the Loop
476 Current an important factor controlling the regional air-sea CO_2 flux. In addition to a
477 relatively high temperature, the Loop Current water is also characterized by low DIC and
478 high alkalinity ([Wang et al., 2013](#) and references therein). The multi-year mean sea
479 surface temperature in [Fig.13b](#) shows persistent warm water mass in the form of the Loop
480 Current, which carries the carbonate characteristics of the Caribbean water (i.e. low DIC
481 and high alkalinity, [Figs. 13e and 13f](#)). Surface $p\text{CO}_2$ in this warm water mass was
482 significantly lower than surrounding shelf waters ([Fig. 13a](#)), making the Loop Current a
483 strong CO_2 sink throughout the year ([Figs.7a-d](#)). Any changes in the Caribbean water's
484 carbonate characteristics will affect the carbon budget in the GoM as well as waters
485 further downstream in the Gulf Stream. This is also illustrated by the high $p\text{CO}_2$
486 difference between the control run and no-biology run in [Fig. 10](#) as well as the poor
487 correlation between the $p\text{CO}_2$ drop (difference between control and no-biology runs) and
488 NCP in the Open Ocean ([Fig. 11b](#)).

489 5.3 Carbon budget estimation and model uncertainty

Z. George Xue 7/1/2016 9:03 AM

Deleted: -

491 Based on our model-simulations, we conclude that the GoM is an overall CO₂
492 sink, taking up $1.11 \pm 0.84 \times 10^{12}$ mol C yr⁻¹ from the air. This estimation is comparable to
493 those based on in situ observations, e.g. 1.48×10^{12} mol C yr⁻¹, (Coble et al., 2010) and
494 0.30×10^{12} mol C yr⁻¹ (Robbins et al. 2014). These recent estimates are in stark contrast
495 to the earlier SOCCR report (Takahashi et al. 2007), which found the GoM to be a CO₂
496 source (1.58×10^{12} mol C yr⁻¹, the GoM and Caribbean Sea combined). In addition, we
497 estimated that the GoM received $\sim 2.18 \times 10^{12}$ mol C yr⁻¹ from rivers, the majority of
498 which was from the Mississippi-Atchafalaya River ($\sim 1.80 \times 10^{12}$ mol C yr⁻¹). These two
499 DIC sources (air: $\sim 1.11 \times 10^{12}$ mol C yr⁻¹ plus river: $\sim 2.18 \times 10^{12}$ mol C yr⁻¹) ~~is~~
500 comparable to the DIC transported out of the GoM by the Loop Current ($\sim 3.30 \times 10^{12}$
501 mol C yr⁻¹, Wang et al., 2013). ~~Such~~ a balance cannot be achieved using the CO₂ flux
502 estimated by Robbins et al., (2014). ~~Nevertheless, here our intent is not to close the~~
503 carbon budget, considering the large uncertainties involved and discussed below. Indeed,
504 the ultimate CO₂ source and/or sink term would be dependent on the relative contribution
505 of both DIC and nutrients to the upper layer of the ocean as well as the biogeochemical
506 alteration therein (Dai et al., 2013).

507 We notice that, during summer months, our model simulated a higher surface
508 pCO₂ than ship measurements on the NGoM Shelf (Fig.6a). As discussed in Section 5.1,
509 a large part of the strong CO₂ degassing was simulated on the Texas Shelf. Yet a close
510 examination of the distribution of available ship measurements indicates that data points
511 on the Texas Shelf are fairly sparse and sporadic (Fig.5), which may partially explain the
512 mismatch between model and ship measurements in Fig.6a. For instance, in the summer
513 of 2010 when more ship measurements were available on the NGoM shelf, both model

Z. George Xue 7/1/2016 9:03 AM

Deleted: largely balance

Z. George Xue 7/1/2016 9:03 AM

Deleted: However, such

516 and observation indicated a high $p\text{CO}_2$ in the summer. In addition, $p\text{CO}_2$ in the
517 Mississippi plume was very sensitive to river DIC inputs. Our specification of riverine
518 DIC (e.g. alkalinity plus 50) was based on limited measurements and may not reflect the
519 true seasonal and inter-annual variability of alkalinity-DIC relationship. The current
520 model resolution (~5 km) may not be high enough to reproduce small-scale circulation
521 patterns associated with the Mississippi River plume. The complexity of the food web
522 and uncertainty in model parameterization (e.g. rudimentarily represented denitrification,
523 remineralization, particular organic matters, the lack of phosphate and silicate
524 components, etc.) warrants further investigation.

525

526 6. Summary

527 A coupled physical-biogeochemical model was used to hindcast surface $p\text{CO}_2$ in
528 the GoM from January 2004 to December 2010. Favorable comparisons were found
529 when validating model solutions against ship measurements on the Gulf-wide scale,
530 indicating that this coupled model can reproduce observed $p\text{CO}_2$ variability in the GoM.
531 Time series of spatially averaged $p\text{CO}_2$ for both shelf and open ocean waters exhibit
532 significant seasonal variability, with high values in August and low values in February.
533 Model-simulated $p\text{CO}_2$ values were elevated by 56 and 88 ppm for the entire Gulf and
534 the NGoM shelf, respectively, when the biological sources and sinks of carbon were
535 disabled (i.e., the no-biology run). Without biological processes, the GoM shifts to a
536 strong carbon source with a outflux rate of $2.10 \text{ mol C m}^{-2} \text{ yr}^{-1}$. Another sensitivity test

537 examining river conditions from the 1904-1910 period (reduced NO_3 and comparable
538 DIC) supported the view that the impact of river inputs were mainly limited to the NGoM

Z. George Xue 7/1/2016 9:03 AM

Deleted: In addition, the

Z. George Xue 7/1/2016 9:03 AM

Deleted: driven by

Z. George Xue 7/1/2016 9:03 AM

Deleted: indicates

542 shelf, which under the conditions of the simulation acted as a CO₂ source with an outflux
543 rate of 0.61 mol C m⁻² yr⁻¹.

Z. George Xue 7/1/2016 9:03 AM

Deleted: could have been

544 The Mississippi-Atchafalaya River plume is the dominant factor controlling the
545 pCO₂ distribution on the NGoM Shelf. Although the NGoM Shelf is overall a CO₂ sink,
546 high surface pCO₂ was simulated in relatively shallow waters, induced by both
547 oversaturated plume water. pCO₂ in the open ocean is controlled largely by the low DIC
548 high alkalinity Loop Current water from the Caribbean Sea.

Z. George Xue 7/1/2016 9:03 AM

Deleted: under those conditions

549 Our model simulations characterize the GoM as an overall CO₂ sink, taking up ~
550 1.11±0.84 × 10¹² mol C yr⁻¹ from the air. Together with the enormous riverine input (~
551 2.18 × 10¹² mol C yr⁻¹), this inorganic carbon influx was comparable with the DIC export
552 through the Loop Current estimated by an earlier study. More accurate model predictions
553 of water column DIC concentration will require more in-situ data for improved
554 specification of riverine DIC inputs, model DIC initial conditions, and further process
555 studies to refine model parameterizations so as to better account for complex carbon
556 dynamics in the coastal ocean.

Z. George Xue 7/1/2016 9:03 AM

Deleted: largely balanced by carbon

557

558 Acknowledgement

559 Research support provided through the National Aeronautics and Space
560 Administration (NNX10AU06G, NNX12AP84G, NNX14AO73G, and
561 NNH13ZDA001N); National Science Foundation (OCE-0752254, OCE-0752110 and
562 OCE-1559279); NOAA Grant NA11NOS0120033. The operational mode of the
563 SABGOM model is located at <http://omgsrv1.meas.ncsu.edu:8080/ocean-circulation/>.
564 Data of daily nowcast/forecast model output is hosted at

Z. George Xue 7/1/2016 9:03 AM

Deleted: refinements in

Z. George Xue 7/1/2016 9:03 AM

Deleted: .

Z. George Xue 7/1/2016 9:03 AM

Deleted: and OCE-0752110); NOAA Grant NA11NOS0120033; GRI GISR grant SA/GoMRI-006 and GOMRI-020, Fund of China National Programme on Global Change and Air-Sea Interaction (Grant Nos. GASI-GEOGE-03 and GASI-04-01-02); and the National Natural Science Foundation of China (Grant Nos. 41476047 and 41106045) is much appreciated.

578 http://omgsrv1.meas.ncsu.edu:8080/thredds/sabgom_catalog.html. Data used in all
579 figures for the hindcast simulation can be obtained by contacting the corresponding
580 author.

581 |

582 **References**

- 583 Aulenbach, B. T., Buxton, H. T., Battaglin, W. T., and Coupe, R. H.: Streamflow and
584 nutrient fluxes of the Mississippi-Atchafalaya River Basin and subbasins for the
585 period of record through 2005: U.S. Geological Survey Open-File Report 2007-1080
586 2007.
- 587 Bauer, J. E., Cai, W.-J., Raymond, P. A., Bianchi, T. S., Hopkinson, C. S., and Regnier,
588 P. A. G.: The changing carbon cycle of the coastal ocean, *Nature*, 504, 61-70,
589 10.1038/nature12857, 2013.
- 590 Benway, H. M., and Coble, P. G.: Introduction. Report of The U.S. Gulf of Mexico
591 Carbon Cycle Synthesis Workshop, Ocean Carbon and Biogeochemistry Program and
592 North American Carbon Program, 63, 2014.
- 593 Cai, W.-J.: Riverine inorganic carbon flux and rate of biological uptake in the Mississippi
594 River plume, *Geophys Res Lett*, 30, 1032, 10.1029/2002GL016312, 2003.
- 595 Cai, W.-J.: Estuarine and Coastal Ocean Carbon Paradox: CO₂ Sinks or Sites of
596 Terrestrial Carbon Incineration?, *Annual Review of Marine Science*, 3, 123-145,
597 doi:10.1146/annurev-marine-120709-142723, 2011a.
- 598 Cai, W.-J., Hu, X., Huang, W.-J., Murrell, M. C., Lehrter, J. C., Lohrenz, S. E., Chou,
599 W.-C., Zhai, W., Hollibaugh, J. T., Wang, Y., Zhao, P., Guo, X., Gundersen, K., Dai,
600 M., and Gong, G.-C.: Acidification of subsurface coastal waters enhanced by
601 eutrophication, *Nature Geosci*, 4, 766-770, 2011b.
- 602 Chassignet, E. P., Hurlburt, H. E., Smedstad, O. M., Halliwell, G. R., Hogan, P. J.,
603 Wallcraft, A. J., Baraille, R., and Bleck, R.: The HYCOM (HYbrid Coordinate Ocean
604 Model) data assimilative system, *Journal of Marine Systems*, 65, 60-83, 2007.

605 Chavez, F. P., Takahashi, T., Cai, W. J., Friederich, G., Hales, B., Wanninkhof, R., and
606 Feely, R. A.: Coastal Oceans, National Climatic Data Center, Asheville, NC, USA,
607 2007.

608 Coble, P. G., Robbins, L. L., Daly, K. L., Cai, W. J., Fennel, K., and Lohrenz, S. E.: A
609 preliminary carbon budget for the Gulf of Mexico, Ocean Carbon and
610 Biogeochemistry News, 3, 1-4, 2010.

611 [Dai, M., Cao, Z., Guo, X., Zhai, W., Liu, Z., Yin, Z., Xu, Y., Gan, J., Hu, J. and Du, C.:](#)
612 [Why are some marginal seas sources of atmospheric CO₂? Geophys Res Lett, 40](#)
613 [\(10\), pp.2154-2158, 2013.](#)

614 Feely, R. A., Sabine, C. L., Lee, K., Berelson, W., Kleypas, J., Fabry, V. J., and Millero,
615 F. J.: Impact of Anthropogenic CO₂ on the CaCO₃ System in the Oceans, Science,
616 305, 362-366, 10.1126/science.1097329, 2004.

617 Fennel, K.: The role of continental shelves in nitrogen and carbon cycling: Northwestern
618 North Atlantic case study, Ocean Sci, 6, 539-548, 2010.

619 Fennel, K., Hetland, R., Feng, Y., and DiMarco, S.: A coupled physical-biological model
620 of the Northern Gulf of Mexico shelf: model description, validation and analysis of
621 phytoplankton [variability](#), Biogeosciences, 8, 1881-1899, 2011.

622 Fennel, K., and Wilkin, J.: Quantifying biological carbon export for the northwest North
623 Atlantic continental shelves, Geophys Res Lett, 36, L18605, 10.1029/2009GL039818,
624 2009.

625 Fuentes-Yaco, C., de Leon, D. A. S., Monreal-Gomez, M. A., and Vera-Herrera, F.:
626 Environmental forcing in a tropical estuarine ecosystem: the Palizada River in the
627 southern Gulf of Mexico, Mar Freshwater Res, 52, 735-744, 2001.

Z. George Xue 7/1/2016 9:03 AM
Deleted: variability

629 Gledhill, D. K., Wanninkhof, R., Millero, F. J., and Eakin, M.: Ocean acidification of the
630 Greater Caribbean Region 1996-2006, *J Geophys Res-Oceans*, C10, 2008.

631 Guo, X., Cai, W.-J., Huang, W.-J., Wang, Y., Chen, F., Murrell, M. C., Lohrenz, S. E.,
632 Jiang, L.-Q., Dai, M., Hartmann, J., Lin, Q., and Culp, R.: Carbon dynamics and
633 community production in the Mississippi River plume, *Journal Limnology and*
634 *Oceanography*, 57, 1-17, 2012.

635 Haidvogel, D. B., Arango, H., Budgell, W. P., Cornuelle, B. D., Curchitser, E., Di
636 Lorenzo, E., Fennel, K., Geyer, W. R., Hermann, A. J., Lanerolle, L., Levin, J.,
637 McWilliams, J. C., Miller, A. J., Moore, A. M., Powell, T. M., Shchepetkin, A. F.,
638 Sherwood, C. R., Signell, R. P., Warner, J. C., and Wilkin, J.: Ocean forecasting in
639 terrain-following coordinates: Formulation and skill assessment of the Regional
640 Ocean Modeling System, *Journal of Computational Physics*, 227, 3595-3624, 2008.

641 Hetland, R., and DiMarco, S.: How does the character of oxygen demand control the
642 structure of hypoxia on the Texas-Louisiana continental shelf?, *Journal of Marine*
643 *Systems*, 70, 49-62, 10.1016/j.jmarsys.2007.03.002, 2007.

644 Hofmann, E. E., Cahill, B., Fennel, K., Friedrichs, M. A., Hyde, K., Lee, C., Mannino,
645 A., Najjar, R. G., O'Reilly, J. E., and Wilkin, J.: Modeling the dynamics of
646 continental shelf carbon, *Annual review of marine science*, 3, 93-122, 2011.

647 Huang, W.-J., Cai, W. J., Castelao, R., Y, W., and Lohrenz, S. E.: Effects of a wind-
648 driven cross-shelf large river plume on biological production and CO₂ uptake on the
649 Gulf of Mexico during spring, *Limnology and Oceanography*, 58, 1727-1735, 2013.

650 Huang, W. J., Cai, W. J., Powell, R. T., Lohrenz, S. E., Wang, Y., Jiang, L. Q., and
651 Hopkinson, C. S.: The stoichiometry of inorganic carbon and nutrient removal in the

652 Mississippi River plume and adjacent continental shelf, *Biogeosciences*, 9, 2781-
653 2792, 10.5194/bg-9-2781-2012, 2012.

654 Huang, W. J., Cai, W. J., Wang, Y., Lohrenz, S. E., and Murrell, M. C.: The carbon
655 dioxide system on the Mississippi River-dominated continental shelf in the northern
656 Gulf of Mexico: 1. Distribution and air-sea CO₂ flux, *Journal of Geophysical*
657 *Research: Oceans*, 120, 1429-1445, 2015.

658 Lee, K., Wanninkhof, R., Feely, R. A., Millero, F. J., and Peng, T.-H.: Global
659 relationships of total inorganic carbon with temperature and nitrate in surface
660 seawater, *Global Biogeochemical Cycles*, 14, 979-994, 10.1029/1998GB001087,
661 2000.

662 Mehrbach, C., Culberson, C. H., Hawley, J. E., and Pytkowicz, R. M.: MEASUREMENT
663 OF THE APPARENT DISSOCIATION CONSTANTS OF CARBONIC ACID IN
664 SEAWATER AT ATMOSPHERIC PRESSURE¹, *Limnology and Oceanography*, 18,
665 897-907, 10.4319/lo.1973.18.6.0897, 1973.

666 Millero, F. J.: Thermodynamics of the carbon dioxide system in the oceans, *Geochimica*
667 *et Cosmochimica Acta*, 59, 661-677, 1995.

668 Milliman, J. D., and Farnsworth, K. L.: River discharge to the coastal ocean : a global
669 synthesis, Cambridge University Press, Cambridge ; New York, 384 pp., 2011.

670 Murrell, M. C., Stanley, R. S., and Lehrter, J. C.: Plankton community respiration, net
671 ecosystem metabolism, and oxygen dynamics on the Louisiana continental shelf:
672 implications for hypoxia, *Continental Shelf Research*, 52, 27-38, 2013.

673 Nixon, S. W., Ammerman, J. W., Atkinson, L. P., Berounsky, V. M., Billen, G.,
674 Boicourt, W. C., Boynton, W. R., Church, T. M., Ditoro, D. M., Elmgren, R., Garber,

675 J. H., Giblin, A. E., Jahnke, R. A., Owens, N. J. P., Pilson, M. E. Q., and Seitzinger,
676 S. P.: The fate of nitrogen and phosphorus at the land sea margin of the North
677 Atlantic Ocean, *Biogeochemistry*, 35, 141-180, 1996.

678 Orr, J. C., Fabry, V. J., Aumont, O., Bopp, L., Doney, S. C., Feely, R. A., Gnanadesikan,
679 A., Gruber, N., Ishida, A., Joos, F., Key, R. M., Lindsay, K., Maier-Reimer, E.,
680 Matear, R., Monfray, P., Mouchet, A., Najjar, R. G., Plattner, G.-K., Rodgers, K. B.,
681 Sabine, C. L., Sarmiento, J. L., Schlitzer, R., Slater, R. D., Totterdell, I. J., Weirig,
682 M.-F., Yamanaka, Y., and Yool, A.: Anthropogenic ocean acidification over the
683 twenty-first century and its impact on calcifying organisms, *Nature*, 437, 681-686,
684 2005.

685 Rabalais, N., Turner, R. E., and Wiseman, W. J. J.: GULF OF MEXICO HYPOXIA,
686 A.K.A. THE DEAD ZONE, *Annual Review of Ecology and Systematics*, 33, 235-
687 263, 2002.

688 Raymond, P. A., Oh, N.-H., Turner, R. E., and Broussard, W.: Anthropogenically
689 enhanced fluxes of water and carbon from the Mississippi River, *Nature*, 451, 449-
690 452, 2008.

691 Robbins, L. L., Wanninkhof, R., Barbero, L., Hu, X., Mitra, S., Yvon-Lewis, S., Cai, W.,
692 Huang, W., and Ryerson, T.: Air-Sea Exchange. Report of The U.S. Gulf of Mexico
693 Carbon Cycle Synthesis Workshop, Ocean Carbon and Biogeochemistry Program and
694 North American Carbon Program, 63, 2014.

695 Sabine, C. L., Feely, R. A., Gruber, N., Key, R. M., Lee, K., Bullister, J. L., Wanninkhof,
696 R., Wong, C. S., Wallace, D. W. R., Tilbrook, B., Millero, F. J., Peng, T. H., Kozyr,
697 A., Ono, T., and Rios, A. F.: The oceanic sink for anthropogenic CO₂, *Science*, 305,

698 367-371, 2004.

699 Sabine, C. L., and Tanhua, T.: Estimation of Anthropogenic CO₂ Inventories in the
700 Ocean, *Annual Review of Marine Science*, 2, 175-198, doi:10.1146/annurev-marine-
701 120308-080947, 2010.

702 Shchepetkin, A. F., and McWilliams, J. C.: The Regional Ocean Modeling System
703 (ROMS): a split-explicit, free-surface, topography-following coordinates ocean
704 model, *Ocean Modelling*, 9, 347-404, 2005.

705 Stocker, T., Qin, D., Plattner, G.-K., Tignor, M., Allen, S. K., Boschung, J., Nauels, A.,
706 Xia, Y., Bex, V., and Midgley, P. M.: *Climate change 2013: The physical science*
707 *basis*, Cambridge University Press Cambridge, UK, and New York, 2014.

708 Sturges, W., and Leben, R.: Frequency of Ring Separations from the Loop Current in the
709 Gulf of Mexico: A Revised Estimate, *Journal of Physical Oceanography*, 30, 1814-
710 1819, 2000.

711 Takahashi, T., Sutherland, S. C., and Kozyr, A.: *Global Ocean Surface Water Partial*
712 *Pressure of CO₂ Database: Measurements Performed During 1957-2012 (Version*
713 *2014)*, Carbon Dioxide Information Analysis Center, Oak Ridge National Laboratory,
714 U.S. Department of Energy, Oak Ridge, Tennessee, 2015.

715 Tian, H., Ren, W., Yang, J., Tao, B., Cai, W.-J., Lohrenz, S., Hopkinson, C., Liu, M.,
716 Yang, Q., Lu, C., Zhang, B., Banger, K., Pan, S., He, R., and Xue, Z.: *Climate*
717 *extremes dominate seasonal and interannual variations in carbon export from the*
718 *Mississippi River Basin*, *Global Biogeochemical Cycles*, 29,
719 10.1002/2014GB005068, 2015.

720 Tsunogai, S., Watanabe, S., and Sato, T.: Is there a "continental shelf pump" for the

721 absorption of atmospheric CO₂, *Tellus B*, 51, 701-712, 1999.

722 Uppström, L. R.: The boron/chlorinity ratio of deep-sea water from the Pacific Ocean,
723 *Deep Sea Research and Oceanographic Abstracts*, 1974, 161-162,

724 Wang, Z. A., Wanninkhof, R., Cai, W.-J., Byrne, R. H., Hu, X., Peng, T.-H., and Huang,
725 W.-J.: The marine inorganic carbon system along the Gulf of Mexico and Atlantic
726 coasts of the United States: Insights from a transregional coastal carbon study,
727 *Limnology and Oceanography*, 58, 325-342, 2013.

728 Weiss, R. F.: Carbon dioxide in water and seawater: the solubility of a non-ideal gas,
729 *Marine Chemistry*, 2, 203-215, 1974.

730 Weiss, R. F., and Price, B. A.: Nitrous oxide solubility in water and seawater, *Marine*
731 *Chemistry*, 8, 347-359, 1980.

732 Xue, Z., He, R., Fennel, K., Cai, W., Lohrenz, S., and Hopkinson, C.: Modeling Seasonal
733 and Interannual Variability of Circulation and Biogeochemical Processes in the Gulf
734 of Mexico, *Biogeosciences*, 10, 7219-7234, 2013.

735 Xue, Z., Zambon, J., Yao, Z., Liu, Y., and He, R.: An Integrated Ocean Circulation,
736 Wave, Atmosphere and Marine Ecosystem Prediction System for the South Atlantic
737 Bight and Gulf of Mexico, *Journal of Operational Oceanography*, 8, 2015.

738 Zeebe, R., and Wolf-Gladrow, D.: CO₂ in Seawater: Equilibrium, Kinetics, Isotopes,
739 Elsevier, Amsterdam, 2001.

740 **Tables and Figures**

741 Table 1. Comparison between observed and modeled air-sea CO₂ flux. Observations are
 742 taken from Robins et al (2014), whereas the model results are seven-year (2005-2010)
 743 model mean*.

		Sub-regions					
		Mexico Shelf	Western Gulf	Northern Gulf	West Florida Shelf	Open Ocean	Gulf- wide**
Subregion Area (10 ¹² m ²)		0.18	0.08	0.15	0.15	1.01	1.56
Simulation 1 (control run)*	Spring	0.97±0.29	-0.24±0.59	1.01±0.89	0.28±0.33	1.51±0.41	1.23±0.48
	Summer	-0.96±0.38	-1.69±0.43	-1.42±0.74	-1.26±0.53	-0.33±0.33	-0.62±0.52
	Fall	-0.76±0.45	-1.06±0.34	-0.79±0.63	-1.73±0.67	0.56±0.61	0.06±0.66
	Winter	0.49±0.28	1.62±0.32	2.49±0.70	1.19±0.38	2.44±0.49	2.21±0.40
	Annual	0.19±0.35	-0.34±0.42	0.32±0.74	-0.38±0.48	1.04±0.46	0.71±0.54
Robbins et al., 2014	Annual	0.09±0.05	-0.18±0.05	0.44±0.37	-0.37±0.11	0.48±0.07	0.19±0.08
Simulation 2 (no-bio)	Annual	-2.77±0.36	-2.02±0.36	-1.64±0.68	-1.79±0.36	-2.08±0.39	-2.10±0.46
Simulation 3 1904-1910	Annual	0.08±0.35	-0.77±0.77	0.61±1.07	0.55±0.46	0.86±0.46	0.50±0.65

744

745 *unit: mol m⁻² yr⁻¹, + indicates ocean is an air CO₂ sink; - indicates a CO₂ source to the
 746 atmosphere

747 **Gulf-wide value is a sum of all sub-regions.

748

749 Table 2. Spatial correlation coefficients between $p\text{CO}_2$, sea surface temperature (SST),
 750 sea surface salinity (SSS), dissolved inorganic nitrate (DIN: NO_3+NH_4), dissolved
 751 inorganic carbon (DIC), alkalinity (ALK), and primary production (P-Prod) on the
 752 Louisiana Shelf and in the open ocean (multi-year mean of 2005-2010, control run).

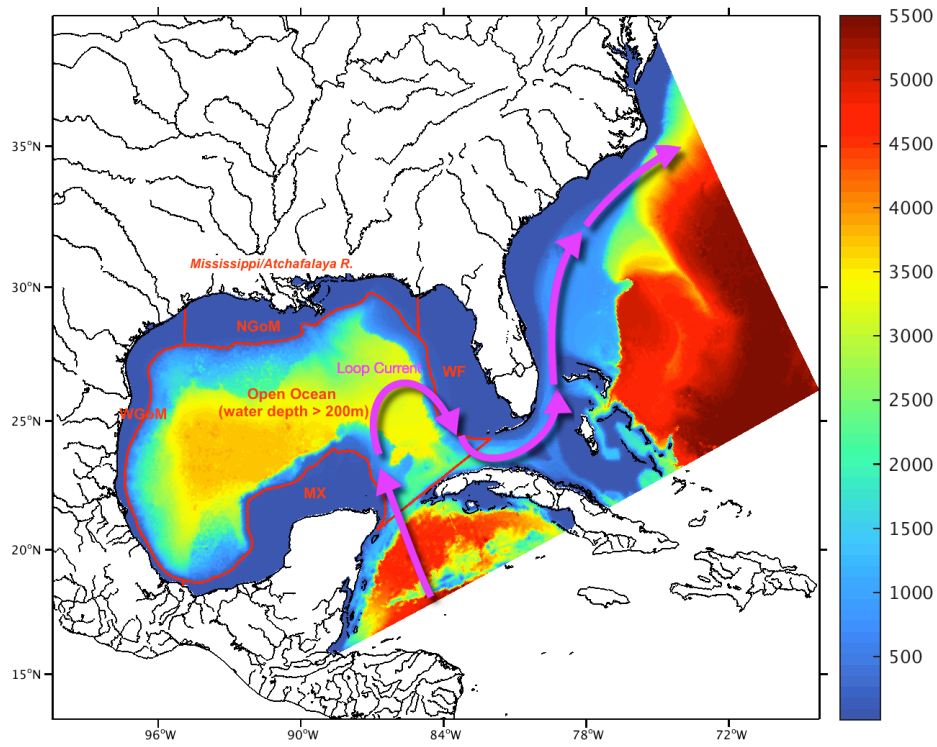
Correlation Coefficient (R value)		SST	SSS	DIC	DIN	ALK	P-Prod
$p\text{CO}_2$ on the NGoM	Spring	-0.24	-0.81	-0.12	0.86	-0.77	0.36
	Summer	0.63	-0.65	0.65	0.66	-0.17	0.35
	Fall	-0.66	-0.87	0.86	0.78	0.17	0.58
	Winter	-0.67	-0.89	0.45	0.89	-0.90	0.23
	Annual	-0.64	-0.82	0.63	0.82	-0.65	0.47
$p\text{CO}_2$ in open ocean	Spring	0.11	0.17	0.76	-0.27	-0.70	-0.41
	Summer	-0.11	-0.11	0.99	-0.29	-0.91	-0.43
	Fall	0.04	0.08	0.96	-0.77	-0.88	-0.76
	Winter	0.04	-0.05	0.75	-0.49	-0.69	-0.55
	Annual	-0.17	0.05	0.93	-0.50	-0.85	-0.59

753

754

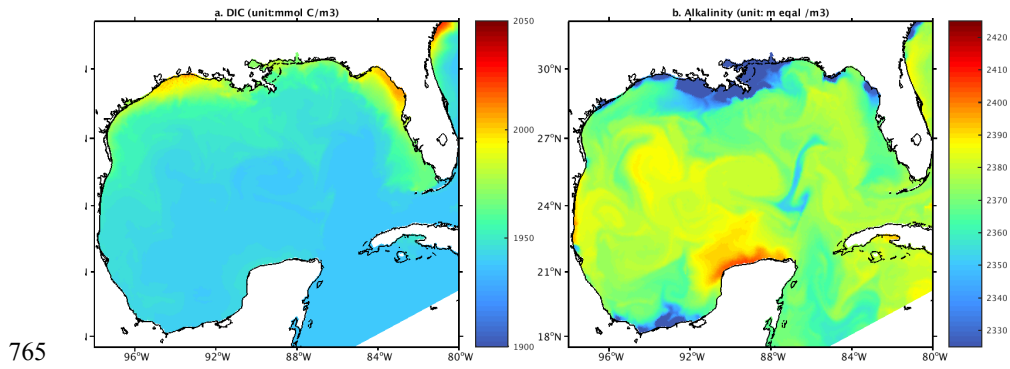
755

756 Figure 1. Domain of the South Atlantic Bight and Gulf of Mexico (SABGOM) ROMS
757 model with water depth in color (unit: m). Also shown are the five sub-regions used in
758 this study, which are Mexico Shelf (MX), Western Gulf of Mexico Shelf (WGoM),
759 Northern Gulf of Mexico Shelf (NGoM), West Florida Shelf (WF), and open ocean. Also
760 shown is a schematic for the Loop Current.
761



762

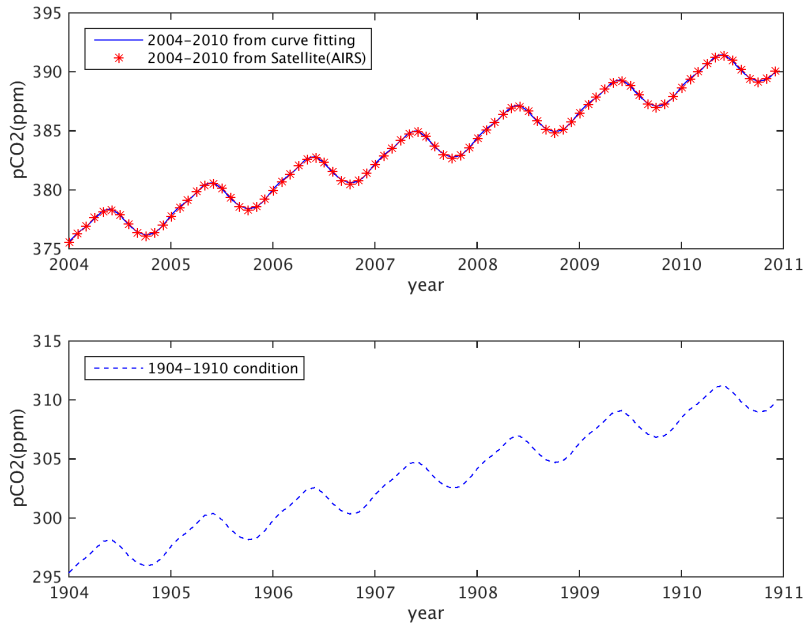
763 Figure 2. DIC and alkalinity initial conditions derived from the empirical relationship by
764 Lee et al. (2000 and 2006).



765

766

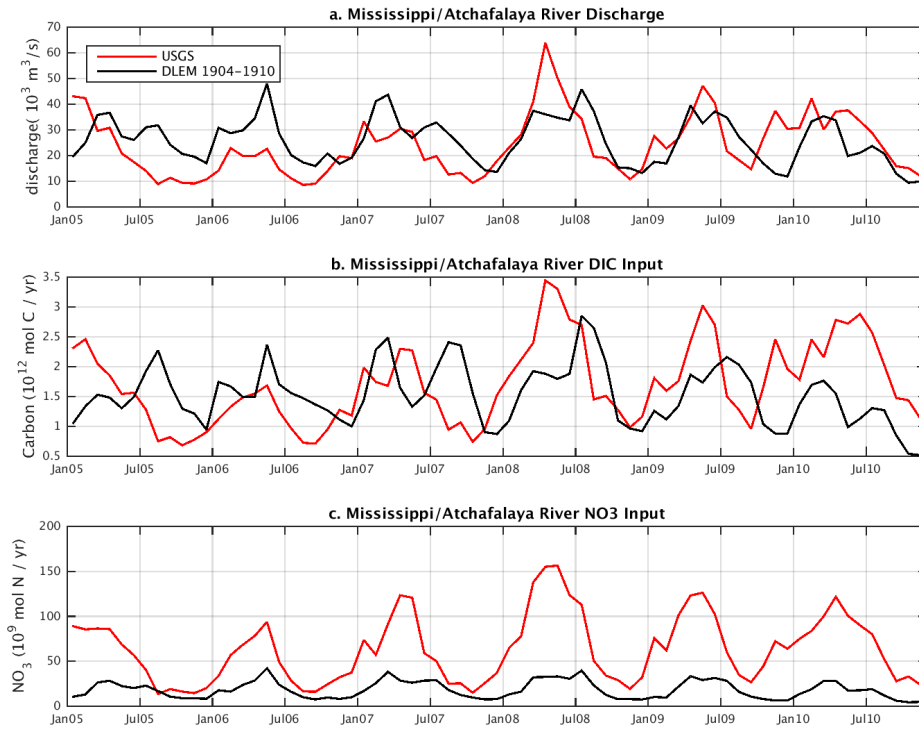
767 Figure 3. Satellite observed monthly pCO_2 (AIRS) averaged over the Gulf of Mexico (red
768 stars) and the pCO_2 air used in model air-sea CO_2 flux calculation (blue line), which is
769 generated using the curve-fitting software CCGCRV.



770

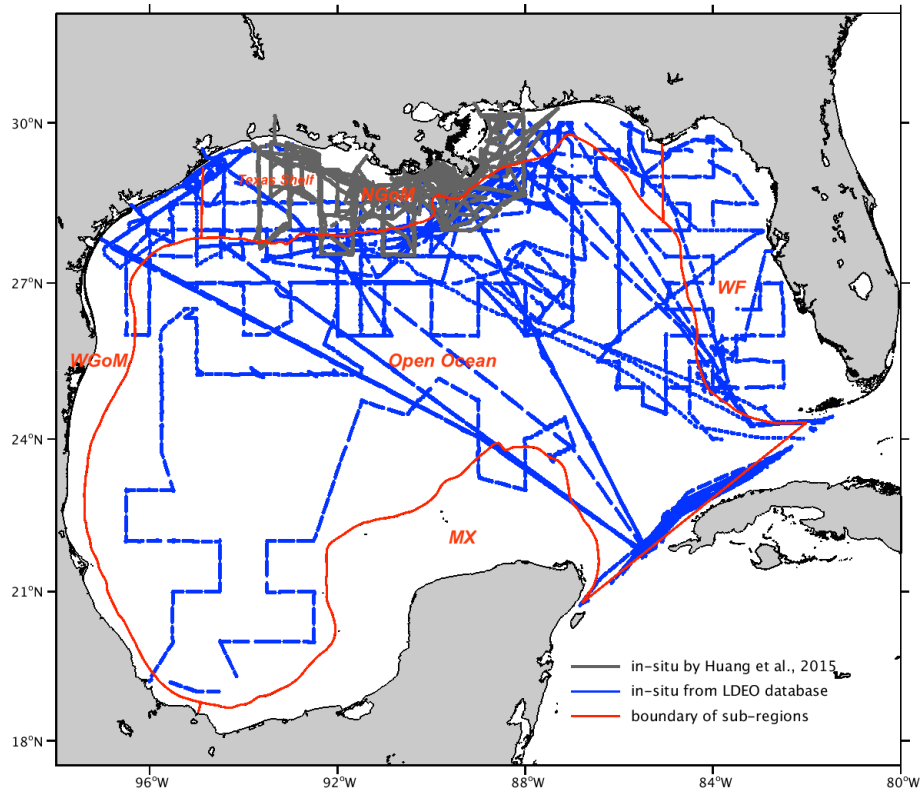
771 Figure 4. Comparisons between the 2005-2010 riverine DIC and NO₃ conditions
772 observed by USGS (red line) and the 1904-1910 river condition simulated by the
773 Dynamic Land Ecosystem Model (black line, [Tian et al., 2015](#)).

774



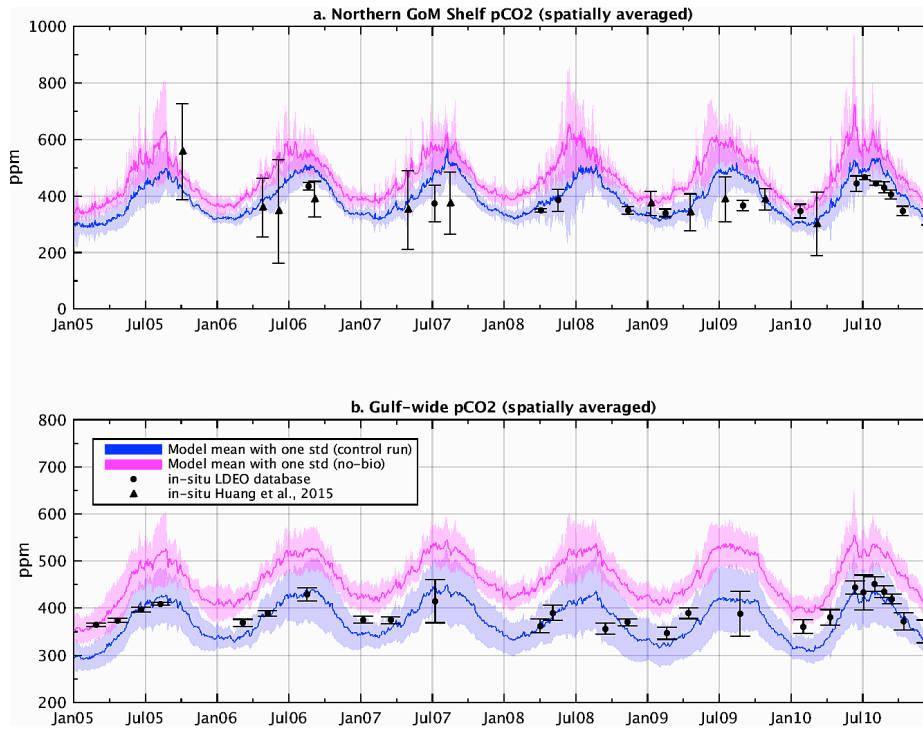
775

776 Figure 5. Locations of in-situ measurements from the LDEO database (blue) and Huang
777 et al. (2015, grey) in the period of 2005-2010.
778



780 Figure 6. Time series of spatially averaged $p\text{CO}_2$ (control run in blue and no-biology run
781 in red) (a) on the Northern Gulf of Mexico shelf, and (b) in the entire Gulf of Mexico,
782 overlaid with in situ observations (in black) from Huang et al. (2015a and b), and
783 Takahashi et al. (2015).

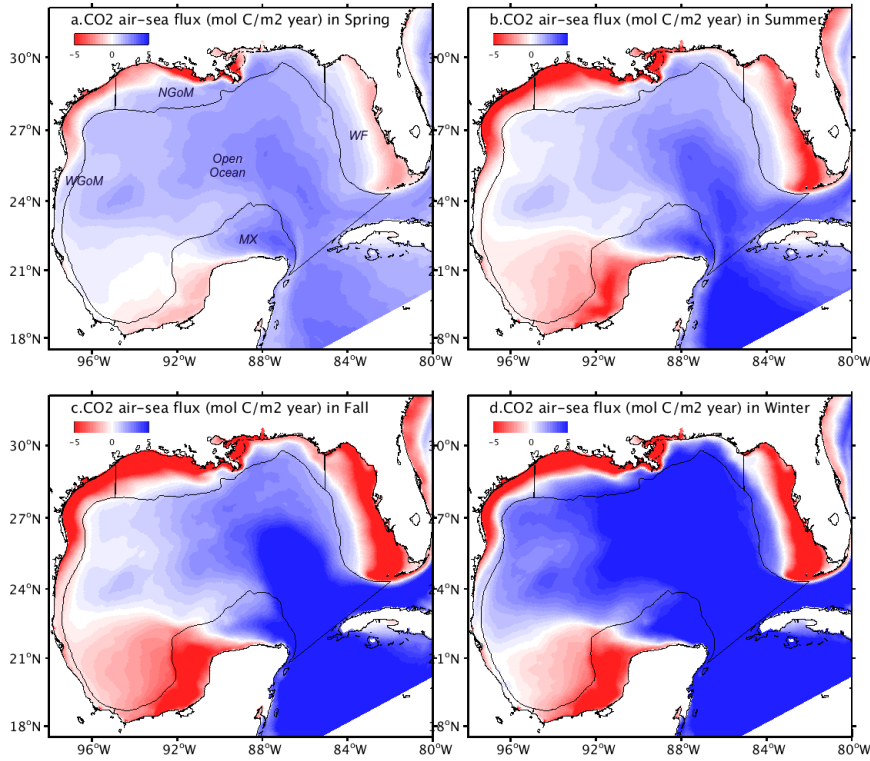
784



785

786 Figure 7. Six-year (2005-2010) model (control run) mean air-sea CO₂ flux in the Gulf of
787 Mexico during (a) spring, (b) summer, (c) fall, and (d) winter. Blue color indicates where
788 the ocean is a sink for CO₂; red color indicates where the ocean is a source.

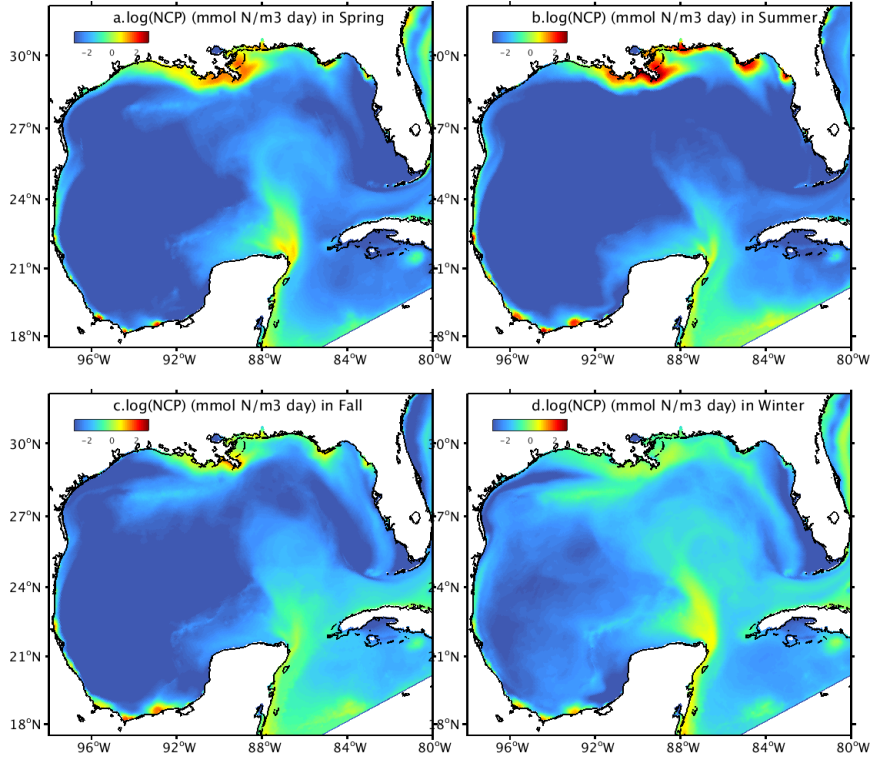
789



790

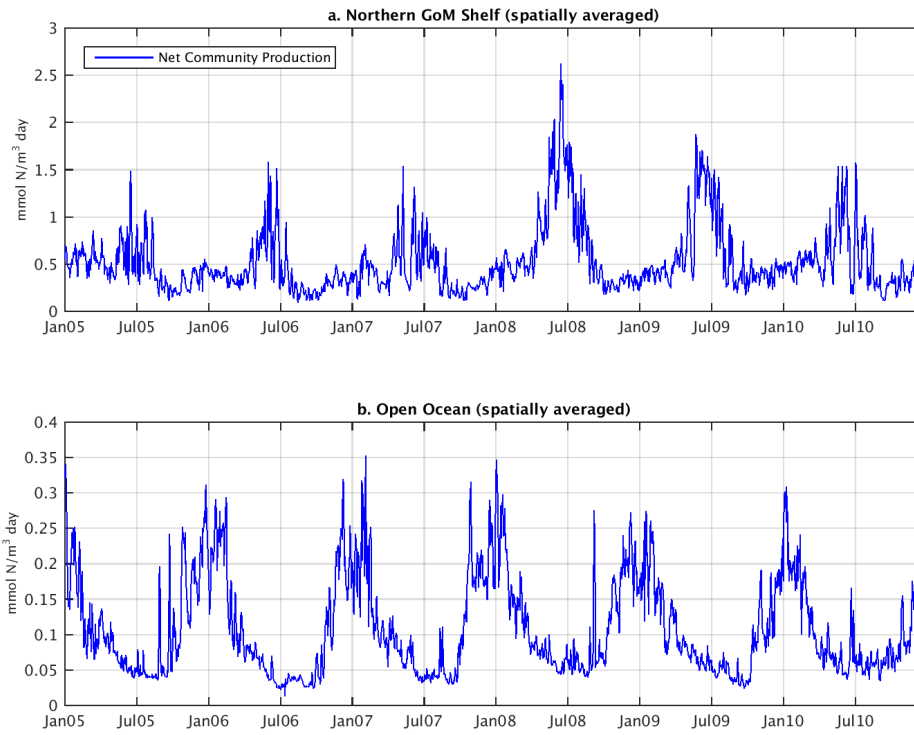
791 Figure 8. Six-year (2005-2010) model (control run) mean surface Net Community
792 Production (NCP) in the Gulf of Mexico during (a) spring, (b) summer, (c) fall, and (d)
793 winter.

794
795



796

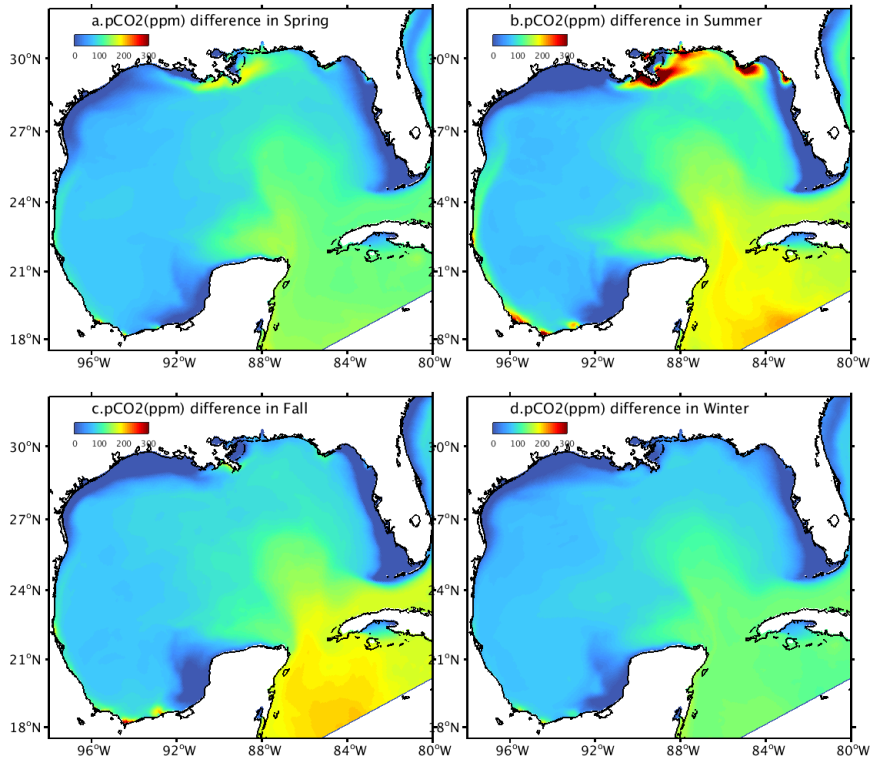
797 Figure 9. Time series of spatially averaged Net Community Production (a) on the
798 Northern Gulf of Mexico shelf, and (b) in the entire Gulf of Mexico (unit: mmol N/m³).
799



800
801
802

803 Figure 10. Multiyear (2005-2010) seasonal mean $p\text{CO}_2$ elevation (No-biology run minus
804 control run, in the Gulf of Mexico during (a) spring, (b) summer, (c) fall, and (d) winter.

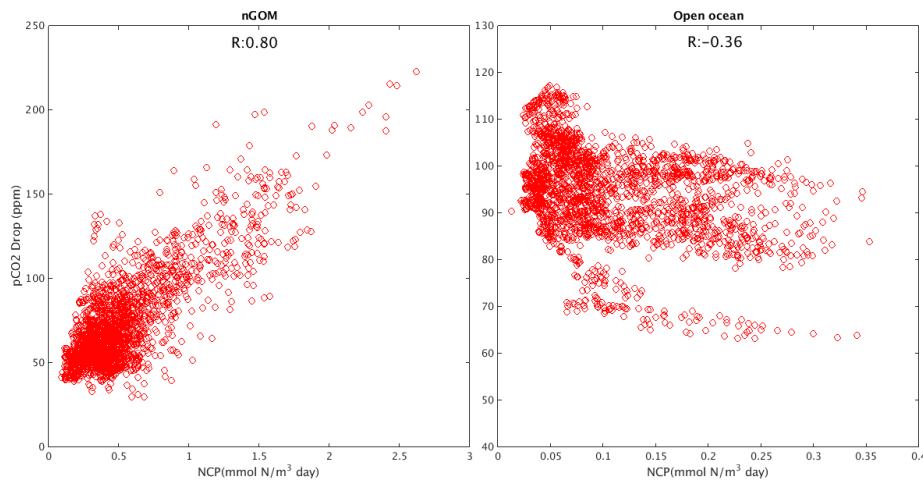
805
806



807

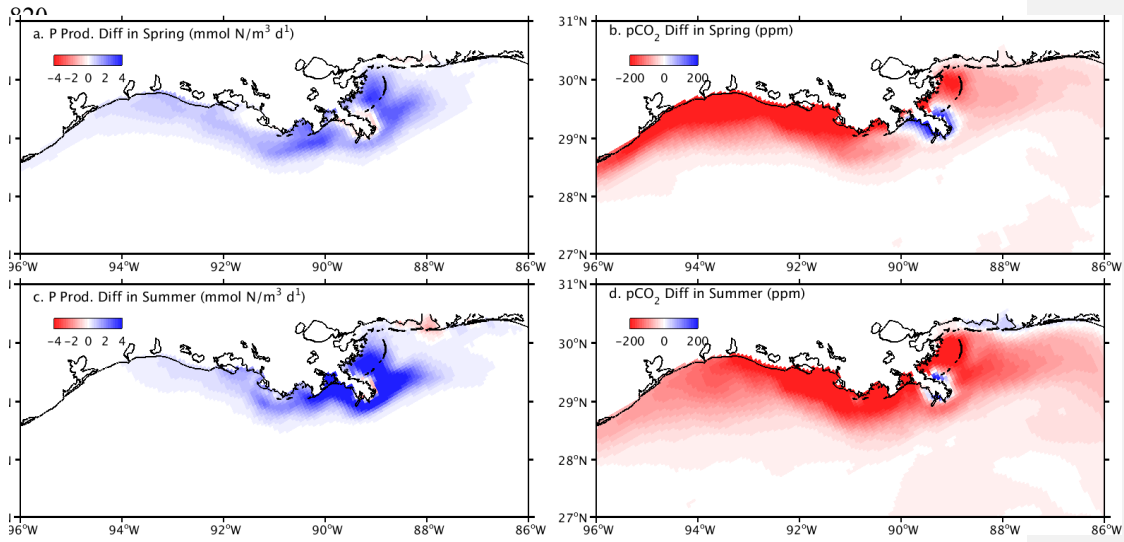
808 Figure 11. Scatter plots of the multiyear mean $p\text{CO}_2$ drop (No-biology run minus Control
809 run) and surface NCP in NGoM (left) and Open Ocean (right).

810
811



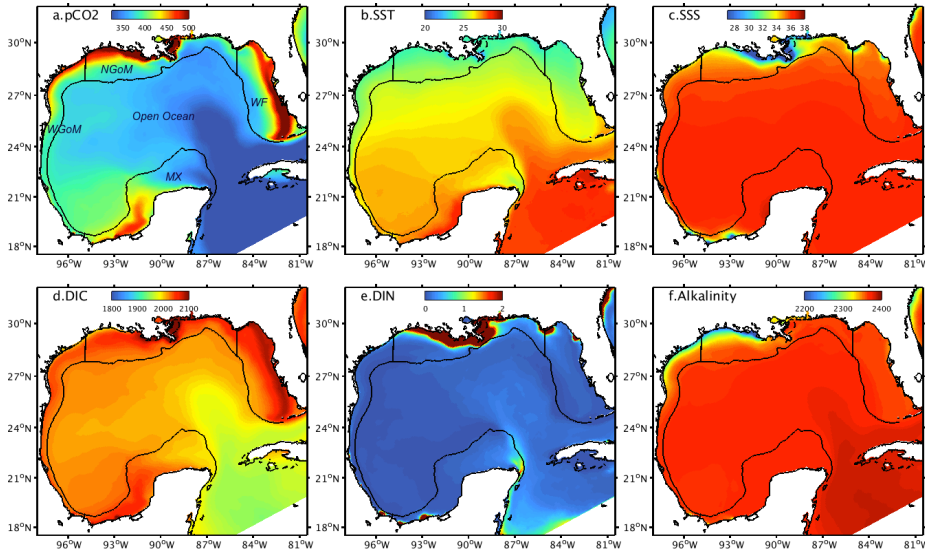
812
813
814

815 Figure 12. Differences in model simulated primary production and $p\text{CO}_2$ between the
816 2004-2010 and the 1904-1910 periods (2005-2010 minus 1905-1910 seasonal mean
817 condition). For a) and c) blue color indicates increased primary production during 2004-
818 2010, for b) and d) red color indicates reduced $p\text{CO}_2$ during 2004-2010.
819



821 Figure 13. Six-year mean (2005-2010) surface conditions simulated by the model for a)
822 $p\text{CO}_2$ (ppm), b) temperature (degree C), c) salinity, d) dissolved inorganic carbon (mmol
823 C m^{-3}), e) dissolved inorganic nitrogen (NO_3+NH_4) (mmol N m^{-3}), and f) alkalinity (mEq
824 m^{-3}).

825



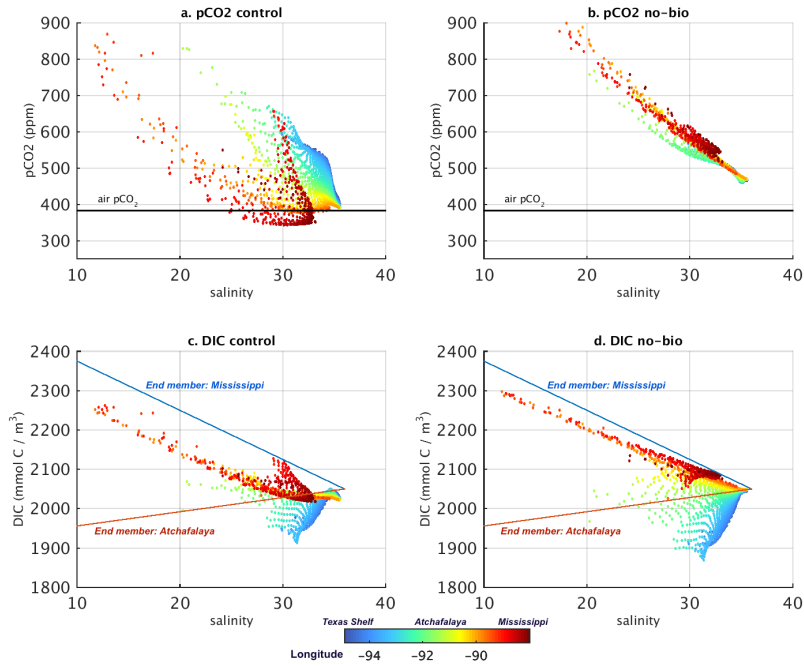
826

827

828

829

830 Figure 14. Six-year (2005-2010) spring-summer mean condition of model simulated sea
831 surface $p\text{CO}_2$ and DIC against salinity for the control run (a and c) and no-biology run (b
832 and d) on the NGoM Shelf; also shown are longitude with colors (note that the
833 Mississippi river delta is located around 89°W and Atchafalaya river delta is located
834 around 91°W). Also shown in c) and d) are conservative mixing relationships for river
835 end members from Cai et al. (2011a).



836

837 **Supplementary Materials**

838 **S1. Calculation of seawater pCO_2**

839 The seawater pCO_2 was calculated following [Zeebe and Wolf-Gladrow \(2001\)](#) as
840 follows:

841

842
$$pCO_2 = DIC * [H^+]^2 / ([H^+]^2 + K_1 * [H^+] + K_1 * K_2) / f \quad (1)$$

843 where DIC is the dissolved inorganic carbon and was given by model input. K_1 and K_2
844 are constant of carbonic acid, $K_1 = [H^+] * [HCO_3^-] / [H_2CO_3]$, $K_2 = [H^+] * [CO_3^{2-}] / [HCO_3^-]$
845 and were calculated following [Millero \(1995\)](#) using data from [Mehrbach et al. \(1973\)](#) as
846 follows:

847

848
$$\log K_1 = 62.008 - 1/T * 3670.7 - \log T * 9.7944 + S * (0.0118 - S * 0.000116) \quad (2)$$

849
$$\log K_2 = -4.777 - 1/T * 1394.7 - \log T * 9.7944 + S * (0.0184 - S * 0.000118) \quad (3)$$

850

851 where in (2) and (3) the T is for water temperature (unit: K) and S is for salinity;

852 The f in (1) is the correction term for non-ideality and was calculated from [Weiss](#)
853 [and Price \(1980\)](#) using equation 13 with 6 values. $[H^+]$ is solved using the 5th order
854 polynomial bracket and bisection method with the following 5 coefficients:

855

856
$$p5 = 1; \quad (4)$$

857
$$p4 = -Alk - K_b - K_1; \quad (5)$$

858
$$p3 = DIC * K_1 - Alk * (K_b + K_1) + K_b * borate + K_w - K_b * K_1 - K_1 * K_2; \quad (6)$$

859
$$p2 = DIC * (K_b * K_1 + 2 * K_1 * K_2) - Alk * (K_b * K_1 + K_1 * K_2) +$$

860
$$K_b * borate * K_1 + (K_w * K_b + K_w * K_1 - K_b * K_1 * K_2); \quad (7)$$

861
$$pI = 2 * DIC * K_b * K_1 * K_2 - Alk * K_b * K_1 * K_2 + K_b * borate * K_1 * K_2 +$$

 862
$$K_w * K_b * K_1 + K_w * K_1 * K_2; \quad (8)$$

863
$$p0 = K_w * K_b * K_1 * K_2; \quad (9)$$

864 where *Alk* is for total alkalinity (unit: milli-equivalent per liter) and was given by model
 865 input; K_w is ion product of water ($[H^+][OH^-]$) and K_b is the constant of boric acid
 866 ($[H^+][BO_2^-]/[HBO_2]$), which were calculated following [Millero \(1995\)](#):

867
 868
$$\ln K_b = -8966.90 + 2890.51 * S^{0.5} - 77.942 * S + 1.726 * S^{1.5} - 0.0993 * S^2 / T$$

 869
$$+ (148.0248 + 137.194 * S^{0.5} + 1.62247 * S$$

 870
$$+ (-24.4344 - 25.085 * S^{0.5} - 0.2474 * S) * \ln T + 0.053105 * S^{0.5} * T) \quad (10)$$

871
$$\ln K_w = 148.9802 - 13847.26 / T - 23.6521 * \ln T$$

 872
$$+ (-0.977 + 118.67 / T + 1.0495 * \ln T) * S^{0.5} - 0.01615 * S \quad (11)$$

873
 874 and borate stands for the concentrations for borate and was calculated following
 875 [Uppstrom \(1974\)](#):

876
 877
$$borate = 0.000232 * S / 1.80655 / 10.811 \quad (12)$$

878

879 **S2. Model initial and boundary condition setup for Dissolved Inorganic Carbon**
880 **(DIC) and alkalinity**

881 The initial and boundary conditions for DIC follow the relationship between DIC
882 and Sea Surface Temperature (SST) for the western (sub)tropical Atlantic waters
883 described in [Lee et al., 2000](#) as follows:

884

$$885 \quad DIC = 1940 + 1.842 * (SST - 29) + 0.468 * (SST - 29)^2 \quad (13)$$

886

887 For alkalinity, we use the relationship among DIC and SST and Sea Surface
888 Salinity (SSS) for the sub(tropical) waters described in [Lee et al., 2006](#) as follows:

889

$$890 \quad Alkalinity = 2305 + 58.66 * (SSS - 35) + 2.32 * (SSS - 35) * (SSS - 35) - 1.41 * (SST - 20) + 0.040 * (SST - 20) * (SST - 20); \quad (14)$$

892

893 **S3. Air-Sea CO₂ flux calculation**

894 The air-sea CO₂ flux was calculated following Wanninkhof (1992) as follows:

895
$$F=K*(pCO_{2\ air}-pCO_{2\ water}) \quad (15)$$

896 where $pCO_{2\ air}$ is the air pCO_2 , and $pCO_{2\ water}$ was calculated from (1); F is the air-sea
897 CO₂ flux (unit: millimole C meter⁻² day⁻¹);

898

899
$$K=kL \quad (16)$$

900 where L is the solubility of CO₂ and was calculated following Weiss (1974) as follows:

901

902
$$\ln L = -60.2409 + 93.4517/T + 23.3585 * \text{Log}(T)$$

903
$$+ S * (0.023517 + T * (-0.023656 + 0.0047036 * T)) \quad (17)$$

904 and the k in (14) is the gas transfer velocity and was calculated using

905

906
$$k = 0.31u^2 (Sc/660)^{-0.5} \quad (18)$$

907 where u is the wind speed at 10 m above sea-level from the North America Regional

908 Reanalysis dataset; Sc is the Schmidt number and was set to

909

910
$$Sc = 2073.1 - 125.62 * T + 36276 * T^2 - 0.043219 * T^3 \quad (19)$$

911

912